2004-02

A Neuromorphic Model for Achromatic and Chromatic Surface Representation of Natural Images

A neuromorphic model for achromatic and chromatic surface representation of natural images

Simon Hong and Stephen Grossberg

February, 2004

Technical Report CAS/CNS-2004-003

Boston University Center for Adaptive Systems
and
Department of Cognitive and Neural Systems
677 Beacon Street
Boston, MA 02215

A Neuromorphic Model for Achromatic and Chromatic Surface Representation of Natural Images

Simon Hong[+] and Stephen Grossberg[*]

Department of Cognitive and Neural Systems
And
Center for Adaptive Systems
Boston University
677 Beacon Street, Boston, MA 02215, USA

Abbreviated title: A Model of Surface Lightness Perception

February 2004

Technical Report CAS/CNS TR-2004-003

All correspondence should be addressed to
Professor Stephen Grossberg
Department of Cognitive and Neural Systems
Boston University
677 Beacon Street
Boston, MA 02215
Phone: 617-353-7858
Fax: 617-353-7755
Email: steve@bu.edu

[+] Present address: Laboratory of Sensorimotor Research, Building 49, Room 2A50, NEI, NIH, Bethesda, MD 20892-4435 USA

[*]SH and SG were supported in part by the Air Force Office of Scientific Research (AFOSR F49620-01-1-0397), the Defense Advanced Research Projects Agency and the Office of Naval Research (ONR N00014-95-1-0409), and the Office of Naval Research (ONR N00014-01-1-0624).

Abstract

This study develops a neuromorphic model of human lightness perception that is inspired by how the mammalian visual system is designed for this function. It is known that biological visual representations can adapt to a billion-fold change in luminance. How such a system determines absolute lightness under varying illumination conditions to generate a consistent interpretation of surface lightness remains an unsolved problem. Such a process, called "anchoring" of lightness, has properties including articulation, insulation, configuration, and area effects. The model quantitatively simulates such psychophysical lightness data, as well as other data such as discounting the illuminant, the double brilliant illusion, and lightness constancy and contrast effects. The model retina embodies gain control at retinal photoreceptors, and spatial contrast adaptation at the negative feedback circuit between mechanisms that model the inner segment of photoreceptors and interacting horizontal cells. The model can thereby adjust its sensitivity to input intensities ranging from dim moonlight to dazzling sunlight. A new anchoring mechanism, called the Blurred-Highest-Luminance-As-White (BHLAW) rule, helps simulate how surface lightness becomes sensitive to the spatial scale of objects in a scene. The model is also able to process natural color images under variable lighting conditions, and is compared with the popular RETINEX model.

Keywords: Surface perception, Lightness, Anchoring, Retinal adaptation, Color image

1. Introduction

Efficient visual object recognition is facilitated by preprocessing that enables the correct perception of object surface properties, including *reflectance*. Reflectance is the percent of light reflected by a surface in each wavelength. For example, white has about 90% reflectance with no change of composition in wave lengths. A retina or other photodetector receives a luminance signal, which is a product of reflectance and illumination (Hurlbert, 1989). From this luminance signal, a vision and recognition system needs to discount the illuminant to discover the reflectance itself (Helmholtz, 1866). The perceived reflectance as the output of this recovery process is called *lightness*.

Retinal preprocessing of visual signals contributes greatly to lightness. These processes include light adaptation and contrast adaptation. Some retinal mechanisms contributing to these adaptations include: (1) Ca^{2+} ion-mediated negative feedback occurring at the photoreceptors (Koutalos & Yau, 1996) and bipolar cells (Nawy, 2000); (2) bleaching of photopigments (Dowling, 1987; Fain, 2001); (3) surround negative feedback by the horizontal cell (HC) network (Lee et al., 1999; McMahon et al., 2001; Sterling, 1998; Thibos & Werblin, 1978; Werblin, 1974); and (4) a circuitry switch from cones to rods (Mills & Massey, 1995; Ribelayga, Wang & Mangel, 2002). Such mechanisms enable cells to dynamically change their operating range to adapt to varying lighting situations.

Surface lightness percepts cannot, however, fully be explained by such low-level mechanisms. For example, visual percepts depend upon appropriate interactions between both ON and OFF channel signals that seem to be largely segregated up until cortical area V1 (Dolan & Schiller, 1994; Schiller, Sandell & Maunsell, 1986; Schiller, 1992). The output signals from these low-level processes tend to estimate *relative* measurements of reflectance of the surface in a given display, including relative contrast measurements by center-surround contrast networks (see Section 2.2). Such mechanisms do not, however, exploit the full dynamic range of neurons. There thus remains the problem of remapping the relatively measured signals to absolute lightness percepts that exploit this full dynamic range. This remapping process is called *anchoring* (Gilchrist et al., 1999).

A number of lightness models have been proposed over the years. See Gilchrist et. al. (1999) and Grossberg and Hong (2003) for reviews. No models had previously, however, explained lightness anchoring effects called Articulation, Configuration, Insulation, and the Area Effect (Gilchrist et al., 1999). The present model simplifies a more biologically complete model of these phenomena (Grossberg & Hong, 2003; Hong & Grossberg, 2003) to explain these and other lightness data, and to extend this simplified model to demonstrate an additional competence for processing natural color images under variable lighting conditions.

2. Description of The Model

Figure 1 illustrates the model. The first stage receives a gray-scale version of a color input, and adapts to ambient luminance and spatial contrasts. Using the adapted signal, the next stage generates contrast signals using multiple-scales of antagonistic center-surround processes (see the following descriptions). The retinally-adapted signal also goes via a parallel pathway to the next level unaltered as the luminance signal. The luminance and contrast signals are pooled at the next stage where the signals are rescaled via an anchoring process to assign appropriate lightness values. The anchored signals represent the perceived achromatic lightness in the model. At the final stage, the achromatic lightness is converted into a chromatic version using a simple input-

to-output ratio calculation. This gray-to-color conversion gives the color output the same luminance as the luminance of the corresponding achromatic lightness output.

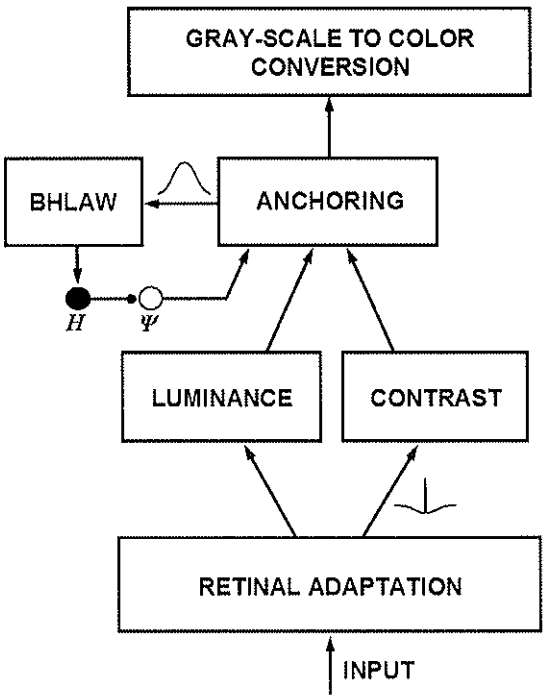

Figure 1. Illustration of the model. Each box indicates an array of cells doing a similar task. Arrow-heads indicate excitatory signals and round-heads indicate inhibitory signals. The narrow Mexican-hat shape curve between the RETINAL ADAPTATION and CONTRAST modules illustrates the one-dimensional shape of the shunting on-center off-surround antagonistic filter for the contrast calculation. The bell-shaped curve between the ANCHORING and BHLAW (Blurred-Highest-Luminance-As-White) modules illustrates the one-dimensional shape of the blurring kernel for anchoring. See the text for details.

2.1 Retinal Adaptation

This stage of the model simulates light adaptation and spatial contrast adaptation of the retina. Some intracellular gating mechanism, such as calcium negative feedback (Koutalos & Yau, 1996), at the outer-segment of the photoreceptor (Figure 2A) is assumed to be responsible for light adaptation in vivo by shifting the operating range of the photoreceptor, as shown in Figure 2B (for a review, see Perlman & Normann, 1998). Spatial contrast adaptation is assumed to happen at the feedback circuit between the inner segment of the photoreceptor and a syncytium of horizontal cells (HCs). The inner segment of the photoreceptor receives the light adapted signal (GATED INPUT in Figure 2A) from the outer segment. It also receives negative feedback from the HC dendrites that are hypothesized to modulate the influx of calcium ions to the axon terminal of the photoreceptor, thus controlling the amount of Glutamate release (GLUTAMATE RELEASE in Figure 2A) from the terminal (Fahrenfort et al., 1999; Verweij et al., 1996). This modulation further adjusts the sensitivity curve of photoreceptors using the spatial context of contrast. Spatial contrast is computed by the HC network using gap junction connections between HCs.

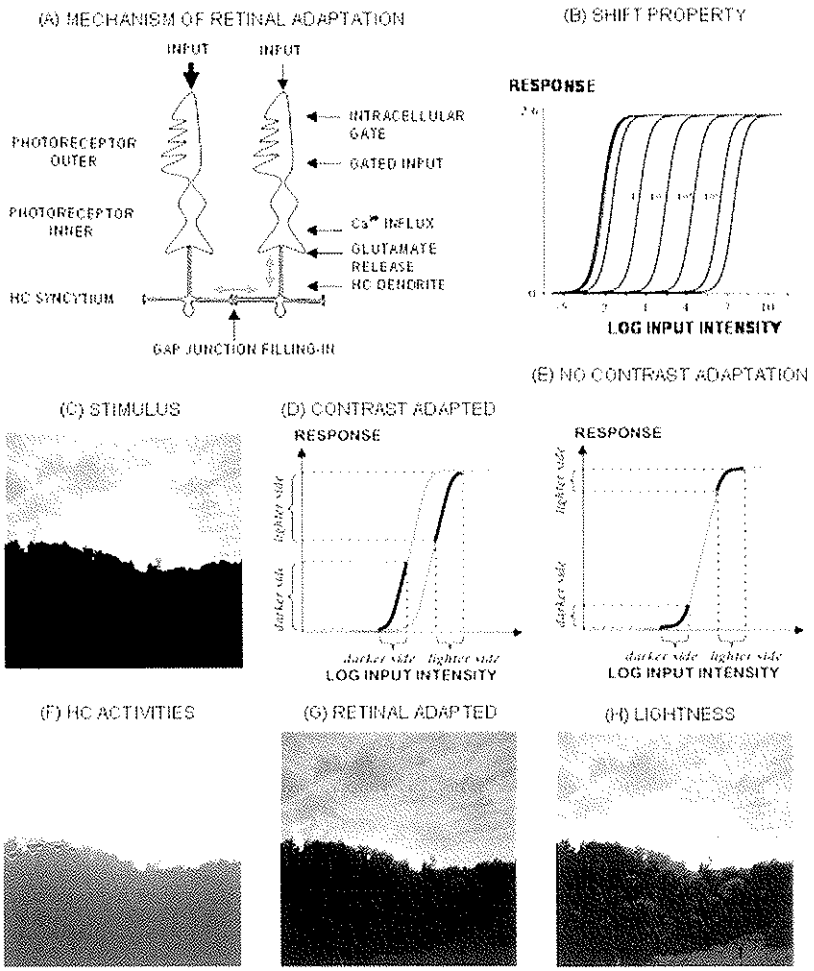

Figure 2. Retinal adaptation. (A) Circuit of retinal adaptation. Two stages of retinal adaptation are implemented: Light adaptation at the outer segment of the photoreceptors and spatial contrast adaptation at the negative feedback circuit between the inner segments of photoreceptors and a syncytium of HCs. Permeability of the gap junctions between HCs decreases as the difference of the inputs to the HCs from the coupled photoreceptors increases. For simplicity, only the connections between nearest neighbors are shown. In simulations, long-range connections are also allowed. The gray bidirectional arrows show the mutual influence between connected units. See the text and Appendix for further details. (B) Light adaptation. The model retina simulates the light adaptation property by automatically shifting its operating range to adapt to the ambient luminance of the visual field. When the luminance is too low, it simulates the physical limit of adaptation (the saturation of shifting on the left end of the graph). Four mean input intensities are shown besides the corresponding curves. The visible 3 leftmost curves have mean luminances of 10^{-4}, 10^{-3}, and 10^{-2} from the left-end, respectively. The rightmost curve has a mean luminance of 10^{7}. (C) Stimulus. (D) Illustration of spatial contrast adaptation. (E) Illustration of retinal sensitivity curve with no contrast adaptation. (F) Steady-state activities of HCs to image (C). The two segregated portions are responsible for the shift of sensitivity curves in (D). (G) Retinally adapted signals. (H) Model output. See the text for further details. [Photo courtesy of Bob Wagner].

It is assumed that the permeability of the gap junctions between HCs decreases as the difference of the inputs to the HCs from the coupled photoreceptors increases. In Figure 2A, for example, the inputs to the network have a steep difference (the thick and thin input arrows). The permeability between the left and right HCs then decreases. When there is not much difference in inputs for connected photoreceptors, the permeability between the HCs remains large. Through this mechanism, the model retina can properly rescale inputs that have too much contrast, such as in Figure 2C. Figure 2F shows the steady-state HC activities in response to the input in Figure 2C. The HCs in the dark and the light image regions hereby deliver different suppressive feedback signals to the photoreceptors. Figure 2D illustrates the two sensitivity curves of the inner-segments of the photoreceptors caused by the two different negative feedback levels of the HC network for the image. Using these two sensitivities, the model retina maps the widely separated input signals (*darker side* and *lighter side* along the abscissa) to sensitive and therefore discriminable portions of the response (*darker side* and *lighter side* along the ordinate). Without this spatial contrast adaptation, the input signals could have been mapped to be too low or high in response, as illustrated in Figure 2E, with a large loss of contrast sensitivity. The rescaled steady-state output of the photoreceptors in Figure 2G shows visible dark and light image regions. Figure 2H shows the final output of the model that computes visible features throughout the scene. See Section 2.4 and Appendix A for details.

To simplify the visual processing, all color inputs are first converted into a gray-scale version using a luminance extraction method from red, greed and blue (RGB) color values (for a review, see Pratt, 1991) before feeding to the retinal adaptation. Reconversion from luminance into color values is discussed in Section 2.4. See Appendix A for mathematical details.

2.2 Multiple-Scale Contrast and Luminance Stage

The retinally-adapted signal is processed by the center-surround contrast stage. For simplicity, the model uses only an on-center off-surround (ON) mechanism with no rectification of negative values. The inclusion of negative values to the contrast signal simplifies the off-center on-surround (OFF) contribution to contrast calculation. While this departure from biology – the omission of OFF channel and inclusion of negative (hyperpolarized) signals – may result in some decrement of contrast in the output, it gives reasonable results in many cases. The model on-center off-surround units are excited by signals falling on the central part of their receptive fields, and suppressed when light falls on the surround of their receptive fields. This antagonistic center-surround mechanism is modeled by a one-pixel excitatory filter for the center and a broad inhibitory Gaussian filter for the surround (Jobson & Woodell, 1995).

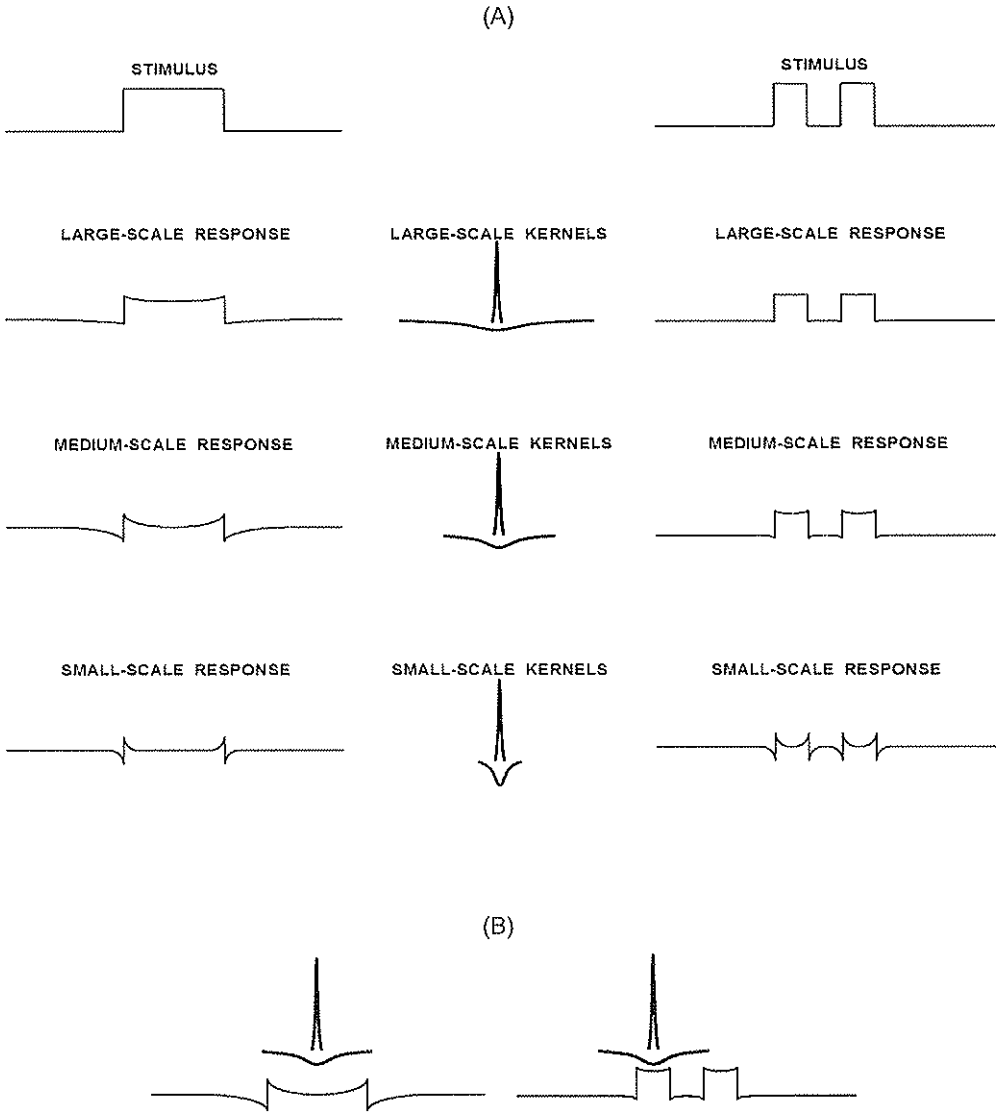

Figure 3. Center-surround processes in multiple scales. (A) One-dimensional illustration of center-surround processes in different spatial scales. The figure shows two stimuli and the corresponding processed signals in different spatial scales in the left and right columns. The center and surround kernels of different spatial scales are shown in the middle column. For simplicity, the sizes of the narrow center kernels are fixed across the scales. (B) Scale-specific signal representation. See the text for further details.

Multiple scales are thus defined by the width of the inhibitory Gaussian filters in the model. These scales contribute with different weights to form a complete representation of the stimulus. For simplicity, three scales are used in the simulation: Small-scale and medium-scale contrast signals and large-scale luminance signals. For simplicity, the size of the sharp center kernel is fixed throughout scales (Grossberg, Mingolla & Williamson, 1995; Mingolla, Ross & Grossberg, 1999; Rahman et al., 1996, 1997). Figure 3 illustrates how the three different scales respond to luminance inputs. As a given surface divides into smaller patches, such as from the

stimulus on the left to the stimulus on the right in Figure 3, medium and large-scale center-surround processes do not fully activate and fully suppress the homogeneous area. This is due to the imbalance between the inputs to the center and the surround sub-receptive fields. Figure 3B illustrates this situation in the medium scale with the center and surround kernels placed on the stimuli. The output of the center-surround process on the left side of Figure 3B shows that the inside of the highest luminance area has been fully suppressed. This is because the center and surround kernels get approximately the same inputs from the highest luminance area and cancel out each other. The figure on the right side of Figure 3B shows an example where there is an imbalance between the inputs to the center and surround kernels (lower average input for the surround compared to the center). The imbalance has caused a high amplitude in the output curve at the highest luminance areas. The model uses this contrast calculation mechanism as part of the Articulation, Configuration, and Insulation effects of lightness anchoring. See Sections 2.3 and 3.5 for further details. Since the large-scale signal tends to represent the luminance signal more veridically (see LARGE-SCALE RESPONSE in Figure 3), we call this the *luminance signal.* This approach differs from the way luminance is computed using ON-OFF channel interactions in the model of Pessoa, Mingolla, & Neumann (1995). In the current model, the retinally adapted signal, which has a large receptive field, serves as the large-scale contrast signal.

One important function of the multiple-scale center-surround design is that the output of this antagonistic process discounts illumination. This is due to the fact that the surround measures the mean luminance over an area using the scale-specific size of the surround, and removes the mean luminance (DC component) from the center activity. This discounting of illumination in multiple scales recovers relative measures of reflectances in a given display.

2.3 Lightness Anchoring and Blurred Highest Luminance As White (BHLAW) Rule

The pooled multiple-scale representation inherits the properties of the retinal adaptation and contrast calculation processes. This representation can, at best, compute relative contrast. For example, a large whiteboard covering more than half of the visual field (Figure 5A) may look middle gray as shown in the Figure 5B. This problem occurs because the normalizing center-surround processes compute just the relative luminance of the center with the surround as the reference point. An anchoring process is needed to remap these relatively defined surface signals into the absolute lightnesses of our percepts.

The lightness anchoring stage rescales the pooled multiple-scale input. At the same time, the activities of the anchoring units are modulated by a feedback signal originating from the anchoring module itself (Figure 1). To achieve the anchoring property, the model first makes a blurred version of the anchoring signal, called the Blurred-Highest-Luminance-As-White (BHLAW) signal (Figure 4A). The model uses this signal to anchor the highest value of the *blurred* pattern to white. This rescaling is achieved by using the BHLAW signal to modulate an automatic gain control process, labeled Ψ (Figures 1 and 4A). Gain Ψ multiplicatively rescales the pooled multiple-scale surface signals. The process H, which inhibits Ψ, becomes activated whenever any BHLAW signal exceeds a threshold that determines the value of white (WHITE in Figures 4B and 4C). This negative feedback circuit achieves the BHLAW rule. One thing to notice is that the inhibition by H on Ψ lowers but does not completely shut off the activity of Ψ, leaving a chance for the BHLAW signals to go beyond WHITE when the bottom up signal is strong enough; for example, a bright light source of some size. In such a case, the BHLAW rule will be violated.

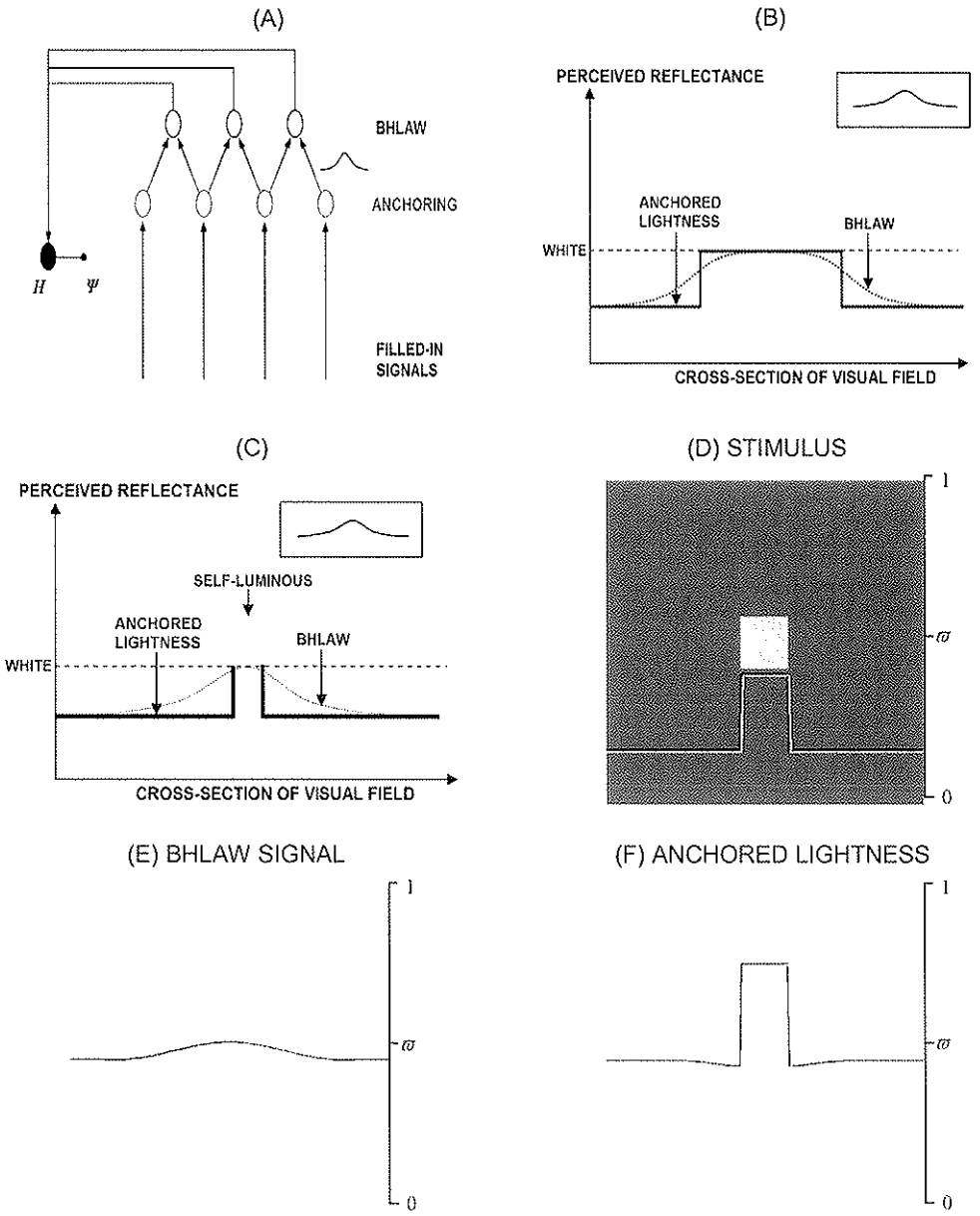

Figure 4. BHLAW rule and Area Effect in a two-field Ganzfeld configuration. (A) Model circuit of lightness anchoring. The activities of the ANCHORING units are locally pooled by BHLAW units to form a blurred version of the ANCHORING signals. The filter used to generate the blurred signals is shown as a bell-shaped figure between the ANCHORING and BHLAW modules. See the text for details. (B) BHLAW rule with a large area of highest luminance. The dashed line indicates the value of WHITE which the blurred highest luminance attains. The thick line (ANCHORED LIGHTNESS) illustrates a 1-D profile of the anchored lightness. (C) BHLAW rule with a small area of highest luminance. (D-F), Two-dimensional simulation of two-field Ganzfeld configuration. D shows the input configuration. F shows the area effect corresponding to the one in C. The curve on each figure represents the activities of the units along the horizontal midline. This convention applies to all the following figures. The scale for the curve is denoted on the right side of each figure.

Figure 4B illustrates this anchoring process with a simple display called the two-field ganzfeld configuration. A ganzfeld is a homogeneous background covering the entire visual field with no other visual cues. In Figure 4B, the BHLAW signal and the highest luminance in the image are both anchored at white. In Figure 4C, the anchored lightness, or unblurred pattern, looks self-luminous because the area of highest activity is not broad enough to span the blurring kernel, so the blurring kernel also averages lower activities as well. As the area of the highest activity becomes smaller, this mechanism predicts that the background will approach WHITE because of the small difference between the highest and background BHLAW signals. In such a case, the anchored lightness will grow until the highest BHLAW signal equals the anchoring value WHITE, which will also bring the background up close to WHITE. Figures 4D to 4F show a 2-D simulation of a two-field Ganzfeld configuration. Note that the highest activity of the BHLAW module in Figure 4E is anchored to white (ϖ). This dependence of lightness on the size of a region is called Area Effect (Gilchrist et al., 1999). The curve in each figure shows the signal profile along the horizontal middle section of the 2-D image. The labels on the right side of each figure indicate the scale of the vertical axis for the curve; in particular, ϖ denotes white.

Figure 5C shows a correct prediction by the model that uses the BHLAW rule. In another example shown in Figure 5F, the model properly handles the light source and the background at the same time. The white curve on Figure 5F shows the profile of the anchored lightnesses along the horizontal section that crosses the light source. The model predicts that the light source will be self-luminous (the peak goes above white, ϖ). The corresponding input taken by a camera uses the Highest-Luminance-As-White (HLAW) rule (Horn 1977; Land & McCann, 1971; Wallach, 1948, 1976), and drove the background to be too dark to recognize.

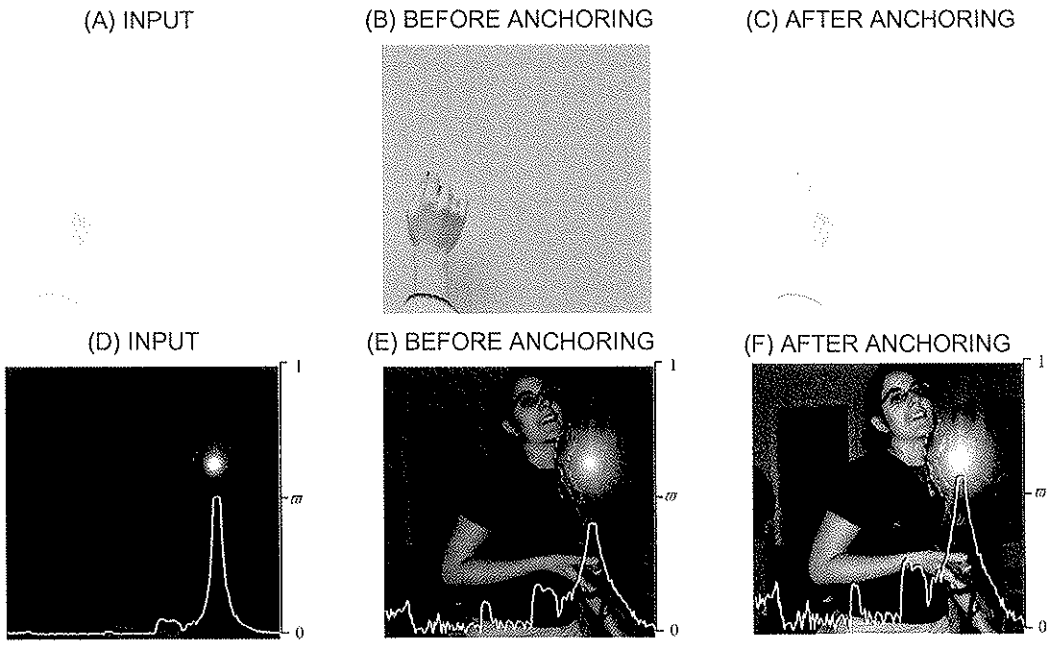

Figure 5. (A) Input. (B) Lightness without anchoring process. (C) Lightness after anchoring with BHLAW rule. (D) Input. (E) Lightness without anchoring process. (F) Lightness after anchoring. The white curve in each figure shows the profile of the signal values along the horizontal section of the image that crosses the light source. The value "ϖ" on the right side of Figure (F) marks the lightness value "white" along the vertical axis. See the text for further details.

2.4 Gray-Scale To Color Conversion

As mentioned in the Retinal Adaptation section, all color input (Red, Green, Blue) values at each pixel point were converted to gray-scale using a luminance extraction method (for a review, see Pratt, 1991) before feeding to the initial retinal stage. After anchoring takes place, the anchored achromatic lightness is reconverted to a chromatic version using a simple input-to-output ratio calculation, as in Figure 6. The process is as follows: First, the input-to-output ratio in the achromatic domain is calculated at each pixel point using the gray-scale input and the anchored lightness output. For example, if the luminance values at the pixel point (x, y) are 1 for the gray-scale input and 10 for the anchored lightness, the input-to-output ratio for the point (x, y) will be 10. This means that the output at the point (x, y) is 10 times more luminous than the input. To generate a color output image that has the same luminances as the gray output, the input-to-output ratio at each gray pixel point is multiplied with the corresponding color input pixel to generate the color output. For example, if the input-to-output ratio is 10 for the pixel point (x, y), the RGB color input values for that point will be multiplied by 10 to generate the output RGB values. This ratio multiplication process guarantees that the outputs of the gray-scale and color images have the same luminance. See Appendix A for mathematical details.

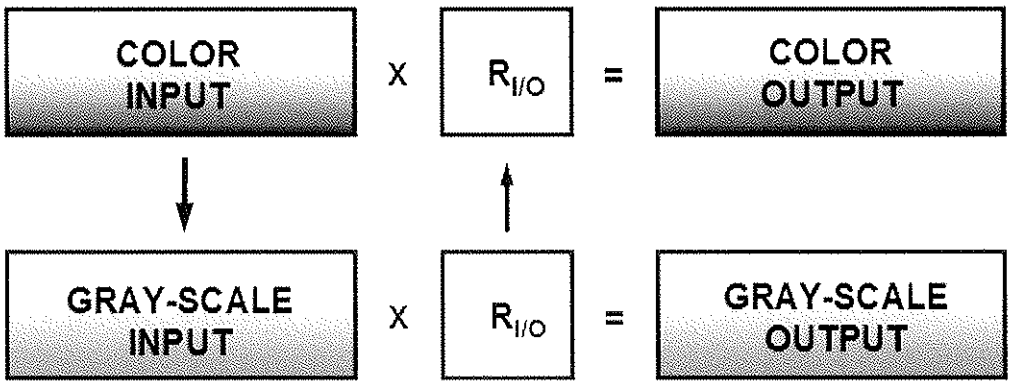

Figure 6. Gray-scale to color conversion. Two parallel gray-scale and color streams are shown. To calculate the color output, the input-to-output ratio ($R_{I/O}$) in gray scale is first calculated at each pixel point. Then, the ratio at each pixel point that represents the input-to-output conversion ratio of luminance is multiplied with the corresponding color input pixel to generate the color output that has the same luminance as the corresponding gray output. Each rectangle represents a grid of pixel values. Each square represents a grid of input-to-output ratios.

3. Results

3.1 Background Light Adaptation

Figure 2B shows the simulated shift property of light adaptation to changing ambient illumination. This property simulates cell recording data of Werblin (1971) and Normann and Perlman (1979). The leftmost curve of the shift property at lower values of background luminance corresponds to the physical limit of light adaptation observed in retinal ganglion cells

(Barlow & Levick, 1969; Enroth-Cugell & Shapley, 1973). The model obeys the Weber law over a wide range of background luminances (Grossberg, 1983). Ambient illumination is removed by divisive intracellular negative feedback signals in the photoreceptors. See Appendix B for the stimuli used for this simulation.

3.2 Discounting the Illuminant

The example in Figure 7 shows that the model discounts the illuminant to discover the reflectance. Figure 7A shows two light patches on a dark background seen in a gradient of illumination. To generate the input, light patches with the same reflectance and a background with a smaller constant reflectance were multiplied by a gradient of illumination. The curves on Figures 7A and 7B show the input intensities and anchored lightnesses along the horizontal midline, respectively. Figure 7B shows the property of illumination discounting: The light patch on the left is almost as light as the one on the right (luminance of the left patch/luminance of the right patch = 0.94), unlike the one in Figure 7A (luminance of the left patch/luminance of the right patch = 0.67). This property comes from the ratio-calculating property of the local contrast units. Figure 7B also shows that, when the gradient of illumination is big enough, the model exhibits a lightness bias where the square patch with higher illumination looks slightly lighter than the one with lower illumination. This property of the model is due to the influence of the large scale that adds a more veridical representation of the stimuli to percepts. This prediction is supported by the observation that, when subjects are asked to decide the perceived reflectance of surfaces, they always give a higher value to the highly illuminated one than the same one with low illumination. (Gilchrist et. al., 1999, p. 826).

The anchored lightness in Figure 7B shows ripples across the background. The reason for this is that the small-scale contrast channel picked up the alias introduced by the non-perfect gradient of illumination in the input. The alias in the display is due to the limited available display values along gradient of illumination. It can be eliminated with a higher resolution representation.

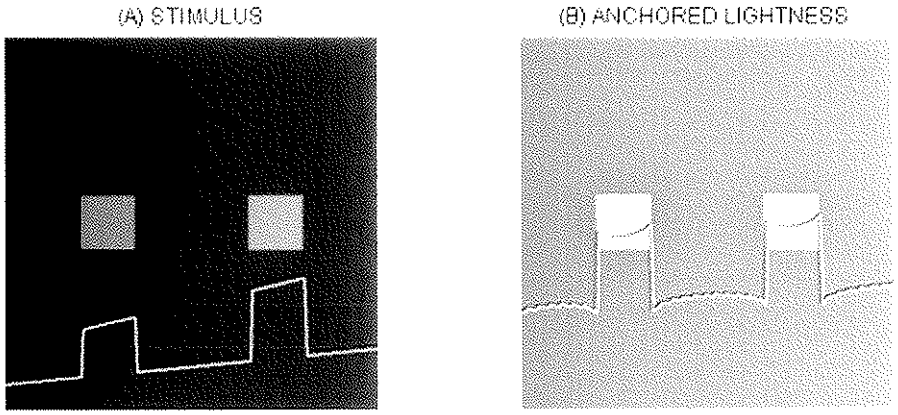

Figure 7. Discounting the illuminant. Unevenly illuminated two light patches with identical reflectance (A.STIMULUS) generate a percept that discounts the illumination (B.ANCHORED LIGHTNESS). However the model also predicts a bit of bias introduced by the illumination gradient (slope of the curve representing the background in Figure A = 0.1). The light patch on the right looks a bit lighter than the left one. The model also picks up the illumination gradient itself using the large scale (slope of the curve representing the background in Figure B $\approx$0.07).

3.3 Simultaneous Contrast

Figure 8 shows a simulation of simultaneous contrast. The two middle gray patches in Figure 8A have identical luminance. In this configuration, small and medium scales calculate local ratio contrasts, and their contribution makes the light square on the dark background look lighter than the one on the bright background even though they have identical luminance (Figure 8B). Since lightness anchoring just rescales the filled-in multiple-scale signals via BHLAW gain control, the anchoring process does not distort the relative lightnesses of the surfaces.

The curve in Figure 8B shows that the anchored surface lightnesses have shallow cusps at the borders of luminance edges. This is due to the nature of the contrast calculation that suppresses information from large homogeneous surface parts (Figure 3). However, the distortion of the image by the cusps is not significant because of the contribution of the large-scale process of the model. Thus, whenever there was a need to measure the lightness of a surface with cusps, the average of the lightness of the surface was computed.

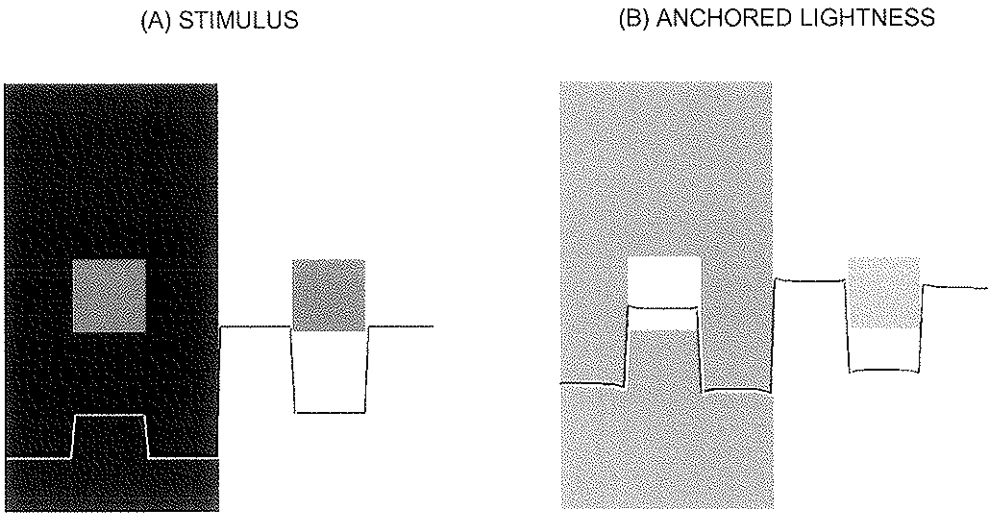

Figure 8. Simultaneous contrast. Two identical square patches on different backgrounds (A.STIMULUS) are perceived differently (B.ANCHORED LIGHTNESS). The one on the dark background looks lighter. Local contrast signals provide the source of this difference.

3.4 Double Brilliant Illusion

Bressan (2001) presented a lightness illusion called the Double-Brilliant illusion (Figures 9A and 9B), wherein a diamond that has less contrast around it (Figure 9B) looks lighter than the one having a high contrast around it (Figure 9A) even though both diamonds have the same luminance (Figure 9C). The model ascribes this phenomenon to the gated negative feedback in the retina. Because the permeability of gap junctions in the horizontal cell (HC) syncytium decreases only where there is a sharp luminance edge in the input, the gradual change of luminance around the diamond in Figure 9B does not block the diffusion of signals across the HC syncytium. The luminance edges around the diamond in Figure 9A do block the diffusion process and segregate the diamond region from the rest of the figure. This gated-diffusion process is simulated in Figure 9D. The segregated and concentrated high signals shown in the diamond region on the left of 9D suppress the corresponding region of photoreceptor outputs. This results in a less active diamond region on the left in Figure 9E compared to the diamond

region on the right. The anchored lightness of the model in Figure 9F reflects this difference and correctly predicts the illusion. This example illustrates that multiple levels of context-sensitive adaptation and recalibration can cooperate to yield lightness percepts. It also allows the possibility that a formally similar negative feedback process that operates at higher cortical processing levels may influence the percept in vivo.

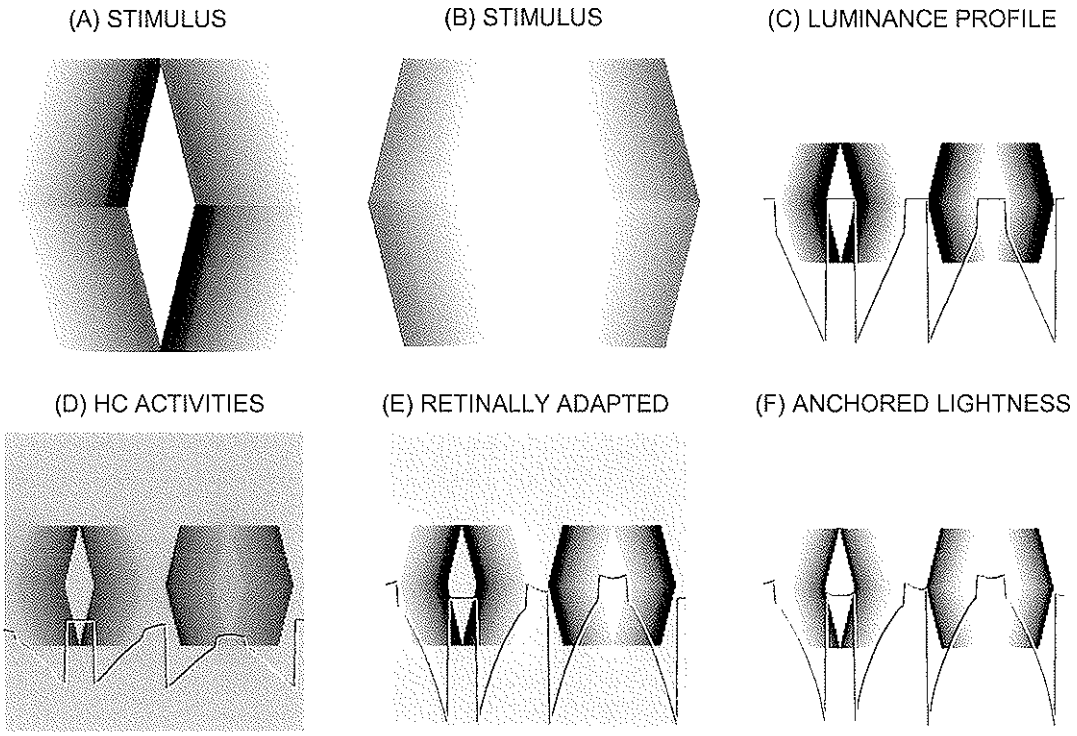

Figure 9. Double Brilliant Illusion. (A-B) Stimuli. Psychophysical experiment shows that diamond part of the stimulus B looks lighter than that of the stimulus A. (C) Stimulus for simulation. (D) Simulated activities of HCs. (E) Steady outputs of photoreceptor inner segments. (F) Anchored lightness. See the text for more details. [Figures (A) and (B) are from Bressan (2001)].

3.5 Anchoring Properties

The model explains the four major effects of lightness anchoring (*Articulation, Configuration, Insulation, Area Effect*) as follows:

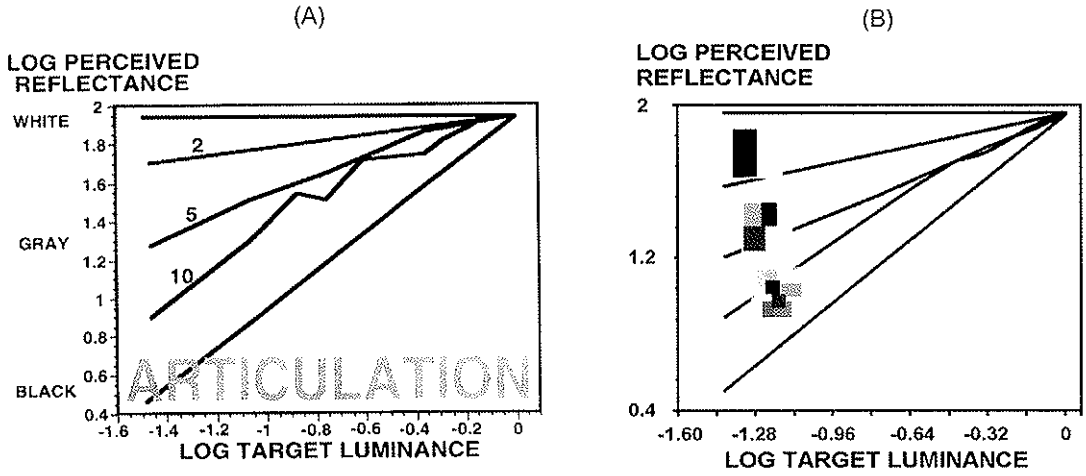

Figure 10. Articulation effect. (A) Data of Articulation effect. As more gray patches are added to a display, the range of perceived reflectance (lightness) widens. In the graph, the widening of the perceived reflectance corresponds to the steeper overall curve as the number of gray level target surfaces increases from one to ten. The widening effect makes the gray patches look darker. The diagonal line shows the perfect situation of lightness constancy. The horizontal line shows the situation where there is just one surface on the Ganzfeld . (B) Simulation results. PERCEIVED REFLECTANCE in the model is ANCHORED LIGHTNESS of the simulation. See the text for details. [Figure (A) is reproduced with permission from Gilchrist et al., (1999).]

Articulation effect: The Articulation effect says that, as a display contains more gray surfaces, the range of perceived lightness widens, or simply, darker ones look darker. The two-, five- and ten-surface Mondrian (2-D arrangement of juxtaposed gray patches) insets in Figure 10B illustrate this experiment situation (see Gilchrist et al., 1999 for a review). The darkening effect of dark surfaces with increasing numbers of distinct gray patches corresponds the steepening data curves in Figure 10A. For example, the black patch (about -1.5 log target luminance, or about 3% of the highest luminance of the display) in the two-Mondrian is perceived as light gray (about 1.7 log perceived reflectance, or 50% of perceived reflectance), while the same black patch in the 5-Mondrian is perceived as middle gray (about 1.3 log perceived reflectance, or 20% of perceived reflectance). A key fact is that, in the experiment, the Mondrian test patches had illumination 30 times that of the dark background resulting in a luminance of 1.4 ftL (foot Lambert). This 30-to-1 foreground-to-background illumination setting is also used in the following Configuration and Insulation effects.

Figure 10B summarizes the model simulation of this effect. As the number of surface patches having different luminances increases in a region, the image contains more high spatial frequencies. In the model, this means that the medium and large spatial scale kernels have less chance to fully activate and suppress the homogeneous area of each patch. Figure 3 illustrates the situation: The divided square luminances on the right cause higher contrast signals in the medium and large-scales compared to the corresponding contrast signals on the left column with a larger square luminance stimulus. The loss of full suppression by each spatial-scale results from the mismatch between the size of the filters and of the patches in the scene. This mismatch at one spatial channel means less suppression, thus more veridical representation for that scale, in

turn causing a more veridical percept. The model explains the jagged part of the 10-Mondrian curve in Figure 10 as a result of the spatial arrangement of gray patches. Similar gray patches can be perceived different depending on the spatial context of surrounding neighbors. The BHLAW process assures that the data remain anchored at white.

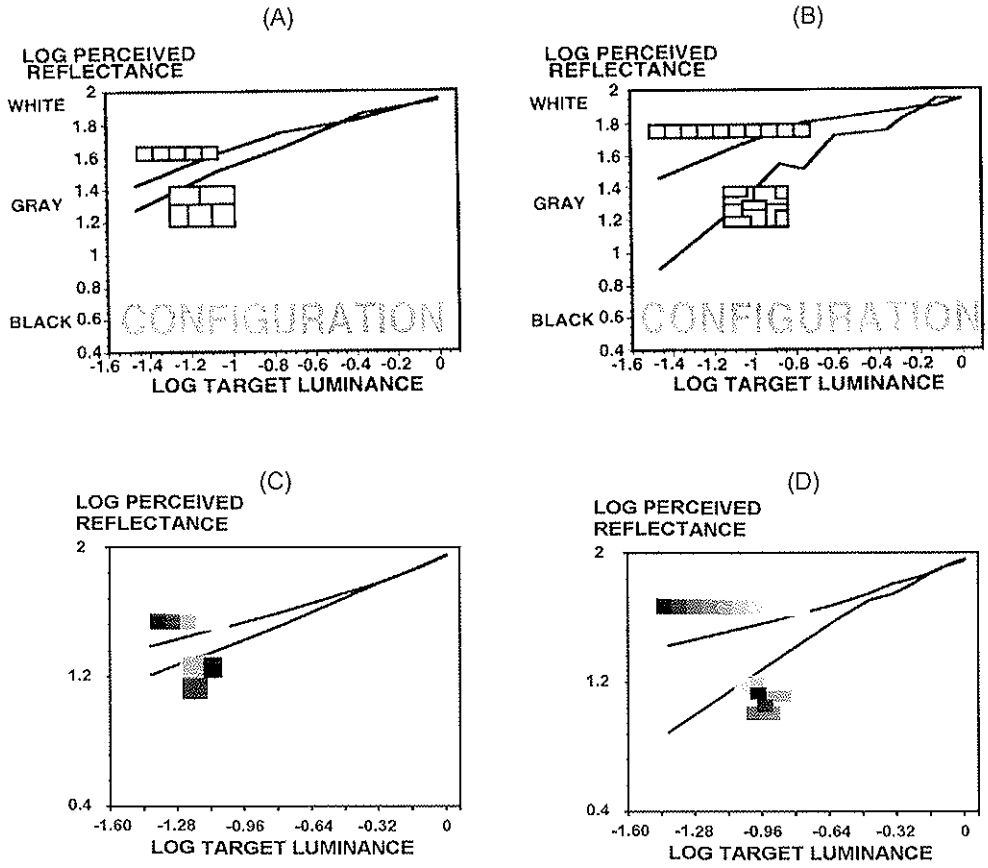

Figure 11. Configuration effect. (A-B) Data of Configuration effect. The lower inset of each figure shows the Mondrian arrangement; the upper inset, the staircase arrangement. The Mondrian arrangement of gray target surfaces widens the range of lightness compared to the staircase arrangement. Comparison of (A) and (B) shows that articulation makes the effect bigger. (C-D) Simulation results, corresponding (A) and (B), respectively. See the text for details. [Figures (A) and (B) are reproduced with permission from Gilchrist et al., (1999).]

Configuration effect: The Configuration effect says that, when a display contains gray surfaces arranged in a Mondrian, a wider range of lightnesses is perceived, or dark ones look darker, than when the same gray surfaces are arranged in a luminance staircase. The Mondrian and the staircase insets in Figure 11C and 11D illustrate this experiment situation (see Gilchrist et al., 1999 for a review). Figure 11B shows an example of the Configuration effect where the black patch (about -1.5 log target luminance) in the 10-staircase is perceived as middle gray (about 1.4 log perceived reflectance, or 25% of perceived reflectance), while the same black patch in the 10-Mondrian looks black (about 0.9 log perceived reflectance, or 8% of perceived reflectance).

Figures 11C and 11D summarize model simulations. The model explains this effect much as it does the Articulation effect: In the Mondrian configuration, since the intermingled luminance patches are arranged in a more radially compact way, the round-shaped surround kernels in the contrast module are influenced by more luminances of surrounding surfaces than with the staircase arrangement. This gives the surround kernels more chance to set the local means (surround activities) to be different from the corresponding center activities. Thus, the increased range of differences between the center and the surround activities results in a bigger range of perceived reflectances for the display. Explained otherwise, if all the adaptation and contrast stage surround activities were the same as their center activities, surround inhibition would drive them all to zero. Also, the radially compact arrangement decreases the distance between different levels of gray patches, thereby inducing stronger lateral inhibition. The dependence of the distance between an inducer and test surfaces has been observed in lightness (Newson, 1958) and brightness experiments (Cole & Diamond, 1971; Fry & Alpern, 1953; Leibowitz et al., 1953), where the darker test surface became lighter with increasing distance from the inducer, an effect interpreted to be due to surround inhibition. Again the BHLAW process anchors the perception of white.

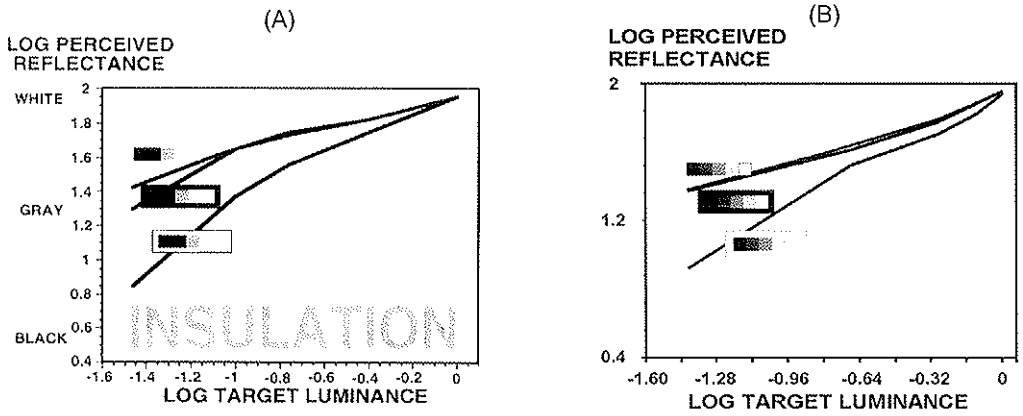

Figure 12. Insulation effect. (A) Data of Insulation effect. Insulation by a white surround widens the range of perceived reflectance. This effect does not seem to happen when a black surround is used for insulation. (B) Simulation results. The model fits the data of configuration effect in the anchoring theory. See the text for further explanation. [Figure (A) is reproduced with permission from Gilchrist et al. (1999).]

Insulation effect: Figure 12 shows the Insulation effect. As with the previous effects, the range of perceived reflectance increases, or dark ones look darker, when the staircase display is insulated by a white surround. The insets in Figure 12A illustrate the experimental displays and data (see Gilchrist et al., 1999 for a review). The black patch in the 5-staircase arrangement is perceived as middle gray (about 1.4 log perceived reflectance), while the same black patch surrounded by white insulation looks black (about 0.8 log perceived reflectance). Figure 12B shows the simulation.

According to the model, a spatial contrast explanation also helps to explain this effect as well: Insulation of gray surfaces with a white surround causes bigger surround inhibition by the introduced bright insulation on the gray surfaces, making them look darker. This results in an

expansion of the range of lightness due to the newly added suppression on dark patches by the surround. Insulation by a black surround, however, may not cause much difference in lightness assessment. This is because the gray surfaces are under illumination 30 times that of the background. Since the gray patches are already not getting much background inhibition, the introduction of black insulation does not significantly change the amount of surround inhibition, thus hardly changing the percept. Once again, the BHLAW process converts these relative lightness activities to an absolute anchored lightness.

Area effect: The Area effect in Figure 13 shows that, in a two-field Ganzfeld situation, as an area other than the area of highest luminance becomes larger than half of the visual field, its lightness approaches white, while the highest luminance area is pushed above white. Figure 13C shows the simulation of this effect.

Comparison of data with the simulation shows that the model closely fits the suggested effect. As explained in the Section 2.3, self-luminosity of a small highest luminance area is explained by the BHLAW rule: When the highest luminance area is smaller than the blurring kernel at the anchoring stage, the blurred filled-in surface signals will have shallower highest activities compared to the un-blurred image (Figure 4C). Since the BHLAW mechanism uses the blurred signals to anchor lightness, the anchored lightness of the highest luminance area will look lighter than white. The case in Figure 4C corresponds to the increasing portions of curves in Figures 13B and 13C. The case in Figure 4B corresponds to the flat regions of the curves in Figures 13B and 13C.

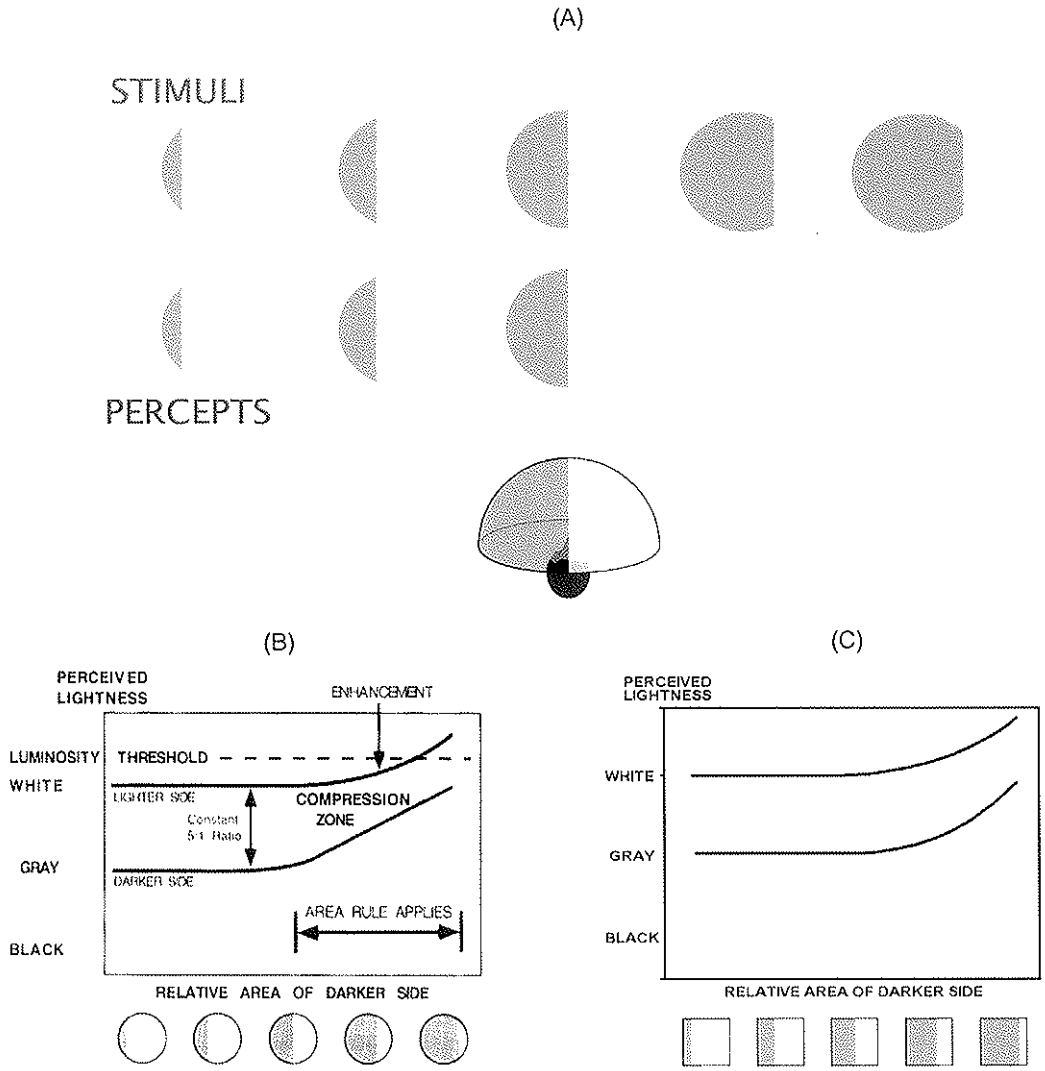

Figure 13. Area effect in divided Ganzfeld situation. (A) Illustration of the experimental settings and the percepts of Area effect. See the text for details. (B) Qualitative illustration of the area effect. As the non-highest luminance area becomes bigger than the half of the visual field, it approaches white, while the smaller area of highest luminance becomes luminous. The divided discs along the abscissa with light and dark surfaces show the configurations of the stimuli. (C) Simulation result of Area effect. The model simulates the concept of the effect quantitatively. The squares along the abscissa with light and dark surfaces show the configurations of the stimuli. See the text for details. [Figure (B) is reproduced with permission from Gilchrist et al. (1999).]

3.7 Natural Color Image Processing

Figure 14 demonstrates the model's ability to process natural color images. Figures 14A, 14D and 14G are inputs, and 14B, 14E and 14H are the corresponding outputs, respectively. The last column shows HC activities for the corresponding inputs. Figure 14B shows the recovery of dark

sides, while preserving the already visible light parts of the scene. The model light adaptation brightens the image; and the model contrast adaptation compresses the range of contrast by applying regionally differing negative feedback. Figure 14B also reveals the distorted signals hidden in the darkness in the input image due to the limited range of sensitivity of the photo-sensors of the camera. Figure 14C shows the HC activities that provide the negative feedback for spatial contrast adaptation. The final lightness assignment, including the luminosity of the candle lights, is achieved by the BHLAW anchoring mechanism of the model. The second and third rows also show some of challenging examples where the model performs robustly.

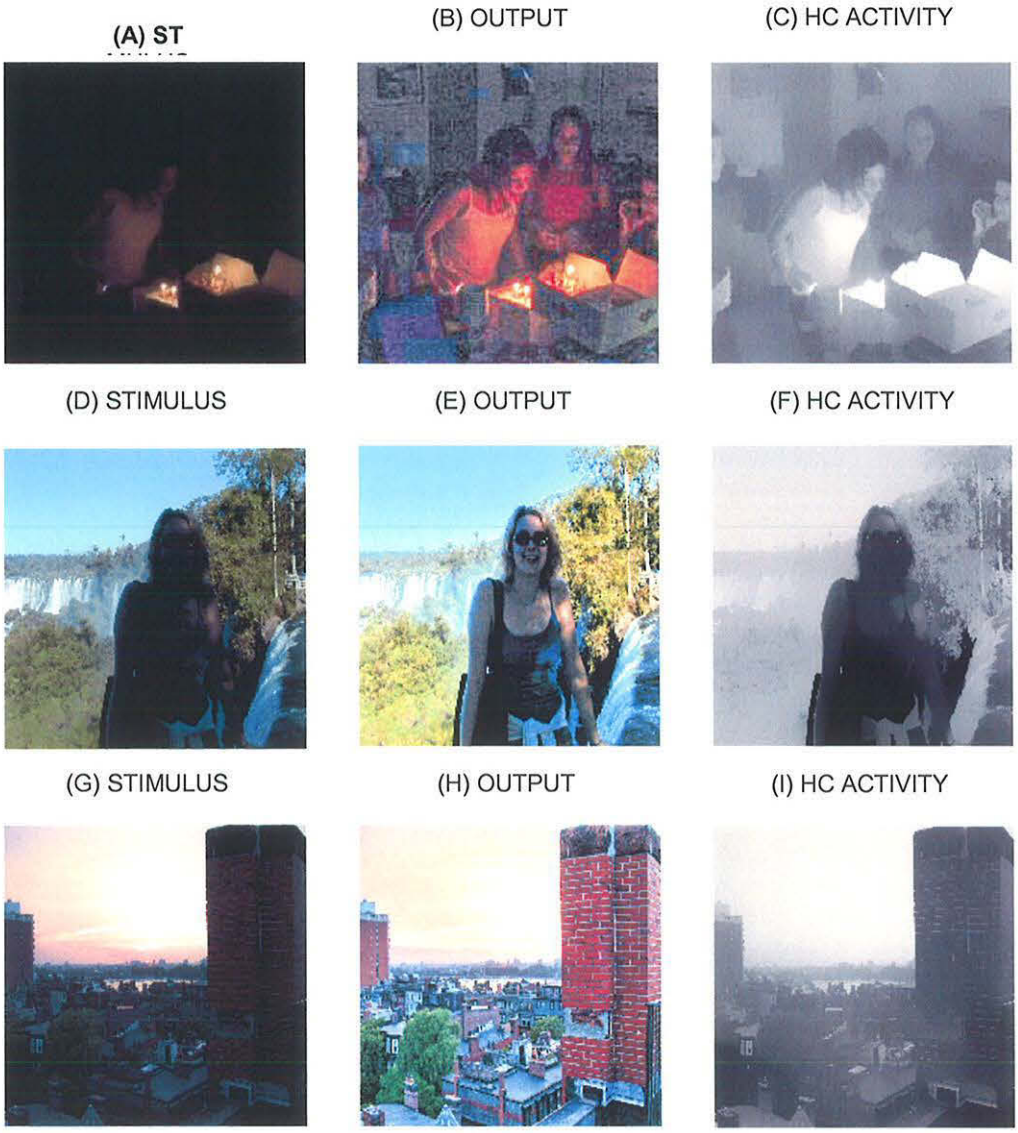

Figure 14. Color image processing. Three examples of color image processing are shown. The first column shows stimuli; the second, the outputs of the model; and the third, the model HC activities for the given images. See the text for details. [Photos courtesy of Arash Fazl and Eric Anderson].

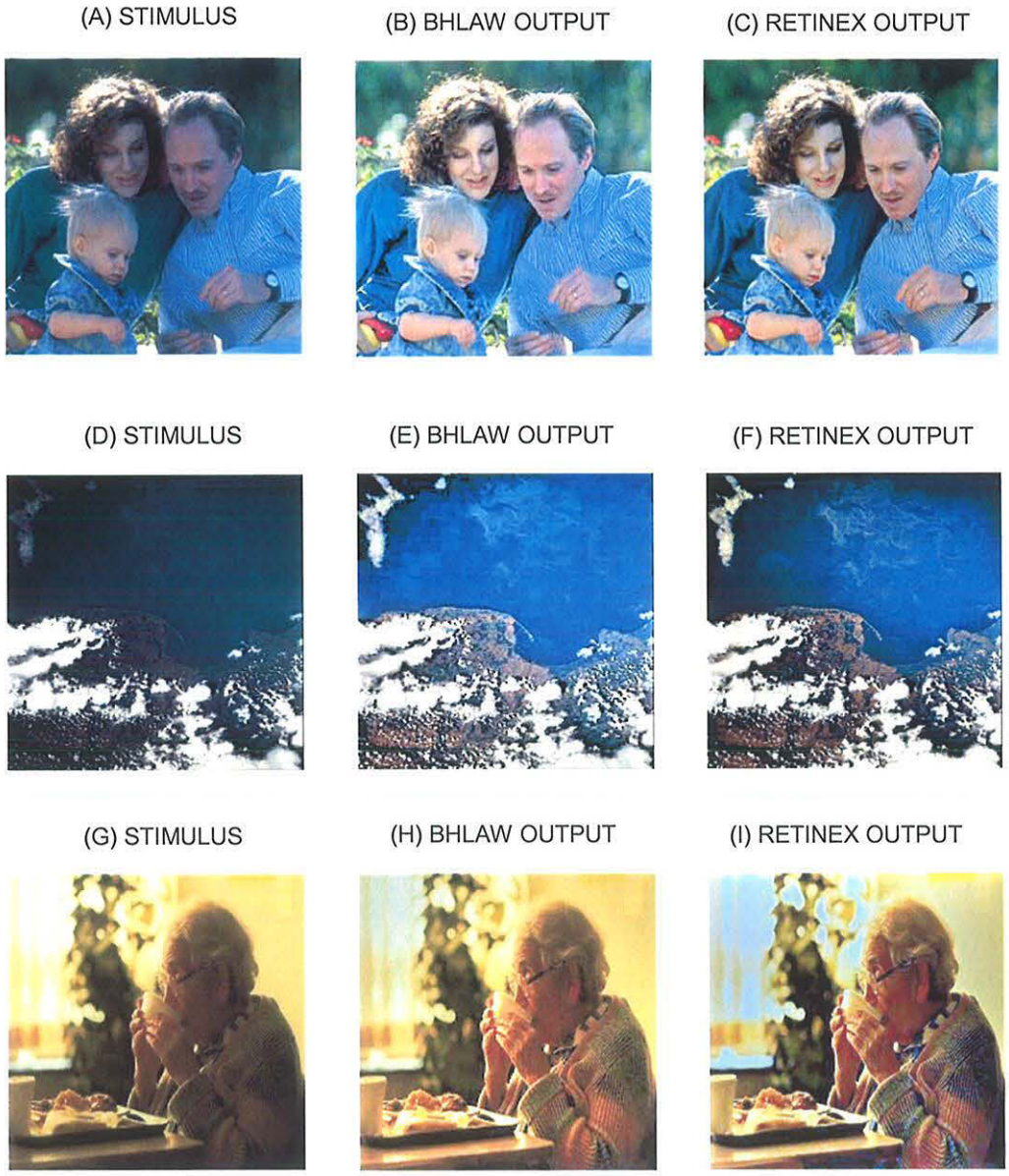

Figure 15. Comparison with Retinex. Three examples of color image processing of the model are compared with the outputs by Retinex. The first column shows stimuli; and the second, the outputs of the model; the third, the outputs of Retinex. See the text for details. [The images on the first and third columns are from NASA Langley Research Center web page].

Figure 15 shows three examples that compare the performance of the BHLAW model with that of the Retinex model of color image processing. Since there are many versions of Retinex designed to be good at different aspects of image processing (see Kimmel et al., 2003 for a review), some of the best known examples from the NASA Langley Research Center web page (http://dragon.larc.nasa.gov/viplab/retinex/) are presented herein. The first row shows an

example that reveals the competence of both of the models. The second row shows an example of remote sensing. While Retinex gives better color contrast across the border, the BHLAW model gives a better scaling of absolute lightness level. For example, the land portion among cloud patches on the right bottom of the image in Figure 15F is too dark to recognize. In contrast, as shown in Figure 15E, the BHLAW model enhanced that part due to the contrast adaptation mechanism of the model that assures a wider signal range of contrast processing. The third row shows an example where Retinex takes off the yellow ambient color (Figure 15I), giving a better estimation of color lightness than the BHLAW model (Figure 15H). However, Figure 15I also shows a known Retinex weakness; namely, over-enhancement of color contrast (see Kimmel et al. (2003) for a review): The bright part along the window looks bluish. In contrast to this, the BHLAW model does not change the composition of wave lengths, as in Figure 15H.

4. Discussion

The BHLAW model that is described in this article generates an anchored representation of surface lightness and color using four signal processing stages: Retinal adaptation first adjusts the sensitivity of retinal cells to the prominent signal range in the input. Using the retinally adapted signals, the multiple-scale center-surround process discounts the illuminant to generate relatively measured reflectances. The third stage anchors lightness to fully use dynamic range. At the last stage, the gray scale lightness is converted to a color version using a luminance-preserving input-to-output transformation. The model simplifies a biological BHLAW model of lightness that was reported in Grossberg and Hong (2003) and extends it to process natural colored images. The following discussion considers the assumptions and limitations of the model.

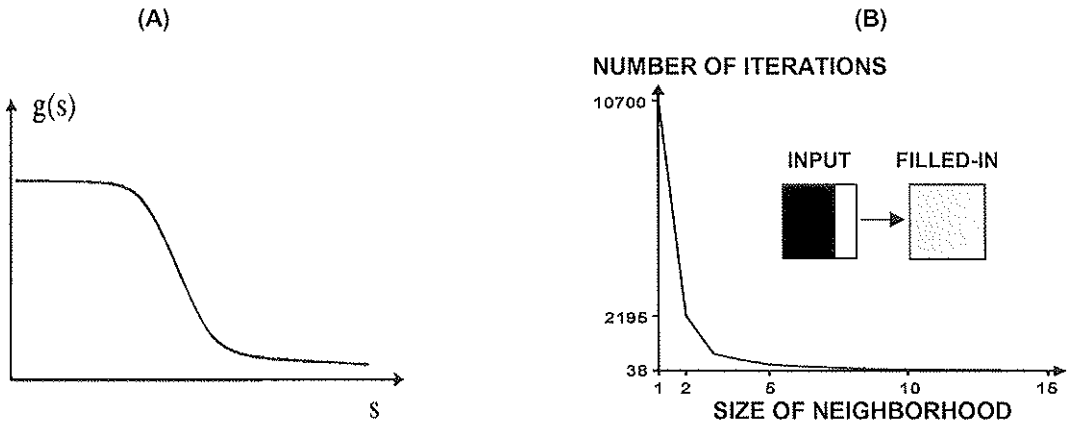

Figure 16. Dynamics of diffusion. (A) Permeability function. The permeability between connected HCs in the current model is a function of spatial contrast as in the model of Perona and Malik (1990). In the model of Perona and Malik, the permeability (g in the graph) between connected units decreases as the differences of signals of the units (s in the graph) increases. (B) Relationship between speed of filling-in and size of neighborhood. As the connectivity expands to a farther neighborhood, the number of iterations needed to homogenize the area decreases rapidly. The insets show the stimulus (INPUT) with signals on the rightmost part of the square (the white region) and the filled-in image (FILLED-IN). [Figure (A) is reprinted with permission from Perona and Malik (1990)].

4.1 Contrast Adaptation

The model assumes that the permeability of gap junctions at connected HCs is governed by an intracellular mechanism, which is in turn controlled by the output of the presynaptic photoreceptors. For example, for two HCs connected by a gap junction, the permeability of the junction decreases as the difference increases between the inputs that the HCs receive from the photoreceptors (Figure 2A). This decrement of permeability with increasing spatial contrast is similar to the one implemented by Perona and Malik (1990) in Figure 16A. Their mechanism is concerned with diffusive filling-in of images and does not include a negative feedback function for automatic gain control. Cohen and Grossberg (1984) and Grossberg and Todorović (1988) implemented gating of signal spread using a boundary signal whose size increases with image contrast. One difference of the current mechanism from these models is that the connections extend farther than just nearest neighbors. These broader connections speeds up the diffusive process. For example, using the Appendix equation (A6) with just nearest-neighborhood connectivity, it takes about 10,000 iterations for a stimulus in Figure 16B (INPUT; 50x50 in dimension) to generate a filled-in output (FILLED-IN in Figure 16B) in case the diffusion is unimpeded (with maximal permeability). The current model has broader connectivity and its filling-in process takes about 100 iterations. Figure 16B illustrates the relationship between the speed of propagation and the size of connected neighborhood. To compare the current long-range diffusive mechanism with the Perona and Malik one, which has no bottom-up input during the iteration of diffusion, only the lateral diffusion component of equation (A6) was used (see Appendix C for mathematical details of the equations and the criteria of filled-in output). The curve in Figure 16B shows that as the connectivity expands to farther neighborhoods, the number of iterations needed to homogenize the area decreases rapidly.

HC receptive field size change due to negative feedback between the photoreceptor and the HC was proposed by Kamermans et al. (1996). Their model emphasized the contribution of negative feedback to determining the length constant of the HCs. Here we show how such negative feedback may clarify how retinal gain control responds to the spatial context of input contrasts.

4.2 Simplification of Contrast Channel

The model simplified the contrast calculation process by removing the OFF (off-center on-surround) contrast channel and letting the negative values of the ON (on-center off-surround) channel contribute to the contrast calculation. This simplification, carried out by not imposing rectification on the output of ON channel, exploits the fact that the profile of the non-rectified output signals of the on-center off-surround contrast calculation [see Appendix equation (A16)] resembles the profile of the rectified signals of on-center off-surround and off-center on-surround channels when they are combined (e.g., equation (31) in Mingolla et al., 1999). As the results of simulations demonstrate, this simplification works: All the contrast-related results predict the correct direction of percepts.

4.3 Area Effect in Natural Images

The area effect tends to be limited to simple Ganzfeld configurations. Gilchrist and his colleagues (1999. p. 802) noted: "Strictly speaking, the rule applies to visual fields composed of only two regions of nonzero luminance. Application of the rule to more complex images remains to be studied." In the model, it is assumed that when the simple Ganzfeld configuration was

tested, the visual system of the subject adapted its multiple scales to compensate for the unusually sparse visual cues. In particular, Sections 2.2 and 4.2 noted that the model incorporates multiple spatial scales which suppress signals that are uniform with respect to each scale. Hence, given the sparse contrasts in the Ganzfeld display, the model would be expected to suppress small scales. Multiple scales were not used in the anchoring module, for simplicity. Such a generalization will be appropriate when the model is generalized to process 3-D scenes. Instead, two different parameter sets were used to explain the area rule: For simple images having just two regions of non-zero luminance (Figure 13C), a bigger Gaussian kernel was used. For all the other, more complex, images with smaller regions, a smaller kernel was applied. See Table 1 for parameters.

4.4 Gray-Scale to Color Conversion

The gray-scale to color conversion used in the model makes an assumption that the visual system may use luminance signals to help anchor color lightness as well as achromatic lightness. This assumption is implemented by a mechanism that modulates the color output to match its luminance to that of the gray-level output of the model. One may also want to ask a question if there is an anchoring rule in color lightness. Recently, Agostini and Castellarin (2003) investigated the question whether a highest luminance in a color display would have a similar effect on color lightness as does a highest luminance in an achromatic display through anchoring. Their finding suggests that there is no clear anchoring-like rule used in the color domain. More investigation is needed to clarify this point. While the current model explains achromatic lightness phenomena quantitatively, it does not address lightness constancy in the color domain; see, for example, the comparison with the Retinex model in Figures 15H and 15I. In particular, it does not process chromatic inputs through opponent and double-opponent mechanisms, cf., Grossberg (1994) and Waxman et al. (1997). Such refinements await additional research on this topic.

Names	Symbols	Values
Upper bound of gain control at photoreceptor	B_z	500
Small-time scale input contribution rate for gain control	C_I	200
Large-time scale input contribution rate for gain control	C_I	600
	B_h	0.05
	B_s	(B^z/C_I)
	a_H	6
	b_H	0.1
Shift of permeability of HC gap junction	β_p	0.08
Steepness of permeability of HC gap junction	λ_p	0.01
Size of connected neighbor for horizontal cell	ϵ_H	13
Surround spatial scales, small, medium	α	3 (for small scale), 14 (for medium scale)
Activation decay	A	0.5
Depolarization constant	B	1
Hyperpolarization constant	D	1
Small, medium, large scale weights	w_s , w_m, w_l	0.2, 0.2, 0.6
Tonic bias of small, medium scales	b_S, b_M	0.001, 0.001
Decay rate for Anchoring	B_A	1
Depolarization constant for Anchoring	C_A	10
Time constant of modulatory unit of anchoring	τ_Ψ	0.01
Depolarization constant of modulatory unit of anchoring	B_Ψ	1.3
Hyperpolarization constant for gain control	ϕ	8
Recharge rate of tonic activity	T_Ψ	1
White	ϖ	0.5
Spatial scale for Anchoring	ζ_A	100 (for the area rule), 4 (for the others)

Names	Symbols	Values
Size of connection range for the surround of center-surround unit	ϵ_E	6 (for small scale), 28 (for medium scale)
Size of connection range for the blurring kernel of Anchoring	ϵ_A	100 (for the area rule), 4 (for the others)
Sizes of various standard kernels	W_E, W_A	0.6, 1
Asymptotic value of color portion in A_{ij}/S_{ij} ratio	Ω	2

Table 1

Appendix A: Model Equations

The model implements 2-D simulations on a 200 x 200 grid that represents the whole visual field.

Retinal Adaptation

The potential s_{ij} at position (i, j) of the outer segment of the retinal photoreceptor is simulated by the equation:

$$s_{ij}(t) = I_{ij} \cdot z_{ij}(t), \tag{A1}$$

where I_{ij} is the input at position (i,j) and $z_{ij}(t)$ is an automatic gain control term simulating negative feedback mediated by Ca^{2+} ions, among others:

$$\frac{dz_{ij}}{dt} = (B_z - z_{ij}) - z_{ij}\left(C_I I_{ij} + C_{\bar{I}}\bar{I}\right); \tag{A2}$$

cf., Carpenter and Grossberg (1981). Parameter B_z in (A2) is the asymptote which $z_{ij}(t)$ approaches in the absence of input. Term $-z_{ij}(C_I I_{ij} + C_{\bar{I}}\bar{I}_{ij})$ describes the inactivation of z_{ij} by the present input I_{ij} and a spatial average $\bar{I}$ of all inputs that approximates the effect of recent image scanning by sequences of eye movements. The equilibrium potential s_{ij} follows from (A1) and (A2):

$$s_{ij} = \frac{B_z I_{ij}}{1 + C_I I_{ij} + C_{\bar{I}}\bar{I}}. \tag{A3}$$

The inner segment of the photoreceptor receives the signal s_{ij} from the outer segment and also gets feedback H_{ij} from the horizontal cell (HC) at position (i, j), as in Figure 2A. HC modulation of the potential s_{ij} of the inner segment of the photoreceptor is modeled by the equation:

$$S_{ij} = \frac{s_{ij}}{B_h \exp(H_{ij}) \cdot (B_s - s_{ij}) + 1}, \tag{A4}$$

where B_h is a small constant, and B_s is a constant close to the value (B_z / C_I). When $B_s = (B_z/C_I)$, perfect shifts of the $\log(I_{ij})$ - S_{ij} curve occur with varying H_{ij} (Figure A1A). When B_s deviates from (B_z/ C_I), compression occurs when $B_s > (B_z/ C_I)$. Expansion occurs when $B_s < (B_z/ C_I)$ in addition to the shift. Thus to prevent expansion, which would mean excitation by the HC negative feedback, B_s needs to be bigger or equal to (B_z/ C_I). Figure A2 shows the 10-Mondrian Articulation situation (see Figure 10) with two values for B_s, one equal to (B_z/ C_I), and the other to $1.2(B_z/C_I)$. This simulation demonstrates that the model is robust under this variation. Compare Figure A2 with the graph in Figure 10B.

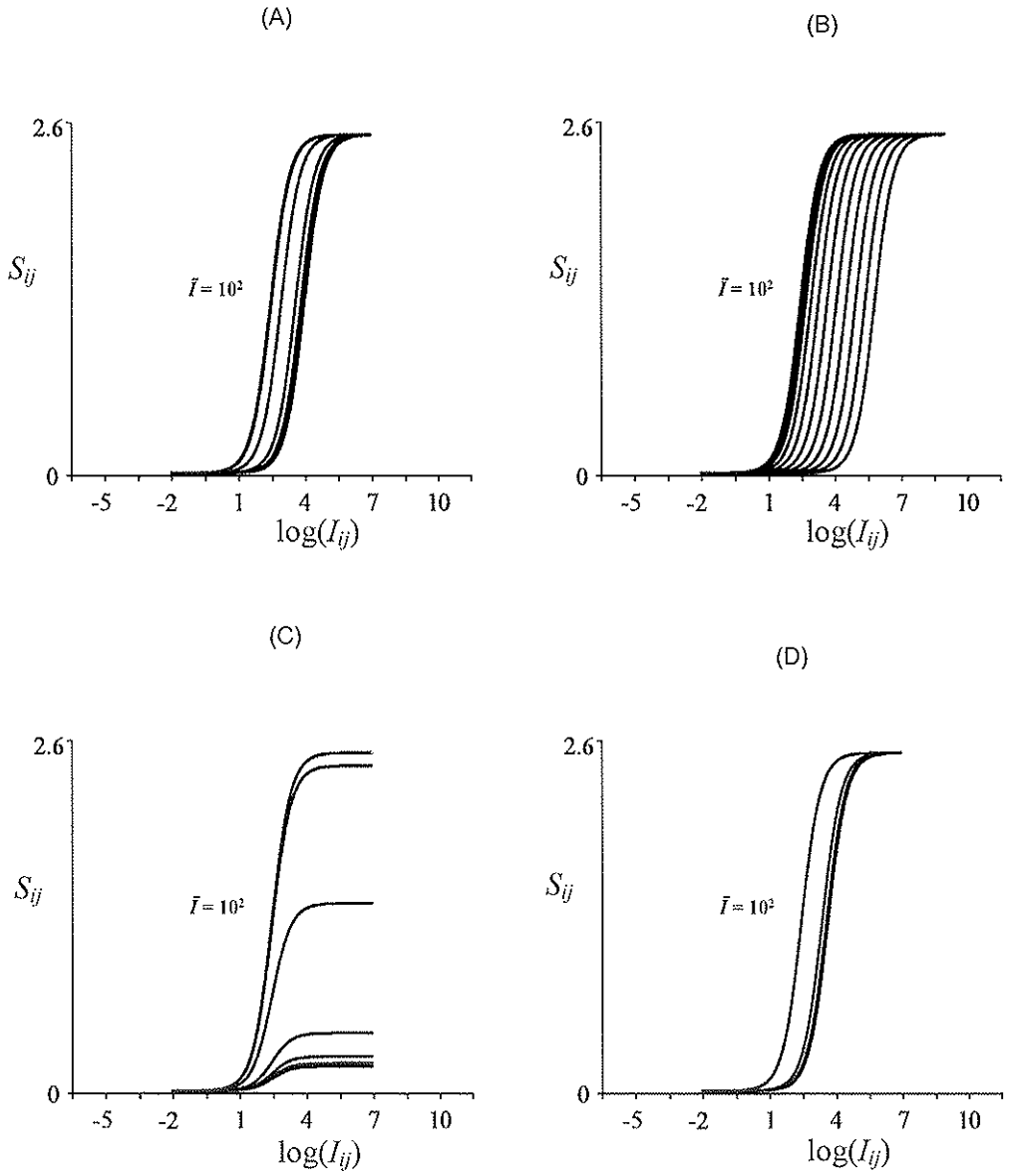

Figure A1. Shift property of spatial contrast adaptation. (A) The graph of S_{ij} as a function of $\log(I_{ij})$ shifts as a function of H_{ij}, first accelerating and later decelerating with growing H_{ij}. These curves are generated using equation (A4) with average luminance $\bar{I} = 10^2$. The same average luminance is used in (B) - (D). The curves from the left to right have h_{ij} values in (A5) of 0 to 0.5 with increment 0.1. The same is true for (C) and (D). (B) Shift property with $H_{ij} = h_{ij}$ in place of equation (A5). The curves show no deceleration. The curves from the left to right have h_{ij} values of 0 to 10 with increment 1. (C) Shift property with no $(B_s - s_{ij})$ term in equation (A4). The curves show a prominent compression. (D) Shift property with $f(H_{ij}) = H_{ij}$ in equation (A4'). The curves do not have the smooth acceleration shown in graph A.

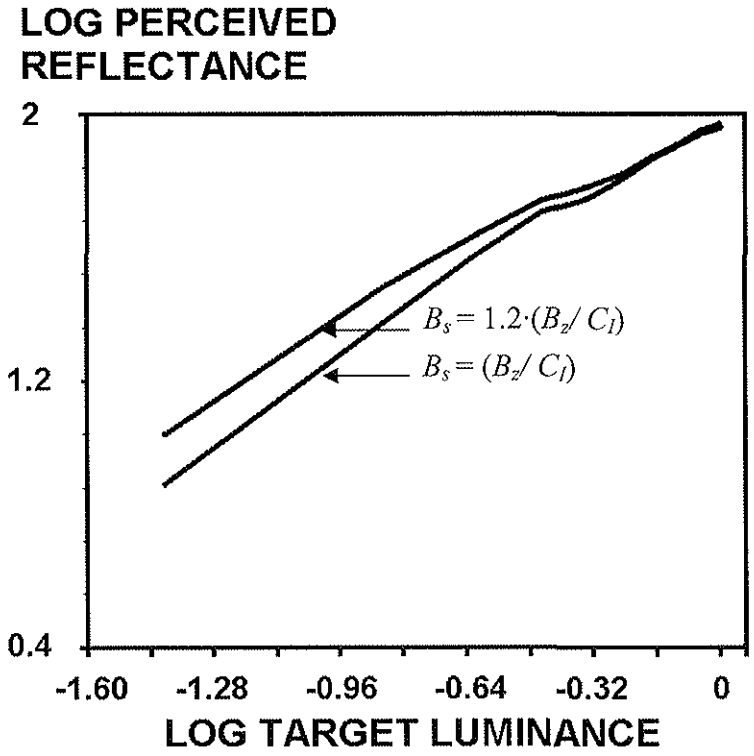

Figure A2. The curves show ten-Mondrian Articulation situation with two values for B_s, one (B_z/C_l), the other $1.2(B_z/C_l)$. While the deviation of 20% from the optimal value shows a bit of compression, the overall quality of Articulation effect remains robust. This demonstrates that the model tolerates a fair amount of fluctuation in the value of the parameter.

Equation (A4) can be generalized as follows.

$$S_{ij} = \frac{s_{ij}}{f(H_{ij}) \cdot (B_s - s_{ij}) + 1} \,. \qquad \text{(A4')}$$

Many increasing functions $f(H_{ij})$ will generate the shift property of S_{ij} as a function of $\log(I_{ij})$. Function $f(H_{ij}) = B_h \exp(H_{ij})$ makes the sensitivity curve shift in an accelerating manner with increasing H_{ij}. Function H_{ij}, in turn, is the sigmoid output of the HC at (i, j) in response to its potential h_{ij}:

$$H_{ij} = \frac{a_H h_{ij}^2}{b_H^2 + h_{ij}^2}, \qquad \text{(A5)}$$

where a_H and b_H are constants. This bounded function causes the amount of shift to decrease as h_{ij} becomes large. The combination of the initial acceleration by the exponential function in (A4) and the later saturation by (A5) causes the S_{ij} curve to accelerate initially and later decelerate with increasing h_{ij}. Figure (A1A) shows an example of this shift property. The leftmost curve represents the S_{ij} curve with $h_{ij} = 0$; the other curves have h_{ij} values of 0.1, 0.2,... , 0.5, respectively. All these curves have the same average luminance $\bar{I} = 10^2$. The shift property is generated at any average luminance $\bar{I}$. Note that the leftmost curve in Figure (A1A) is the same as the curve with $\bar{I} = 10^2$ in Figure 2B. Figure (A1B) shows what happens when $H_{ij} = h_{ij}$ is used

instead of equation (A5), with all other equations the same; it shows no deceleration. Here, h_{ij} values of 0 to 10 were used with increments of 1. Figure (A1C) shows a situation where the term $(B_s - s_{ij})$ in equation (A4) has been replaced by 1; it shows a prominent compression. For this simulation, h_{ij} values of 0 to 0.5 with increments of 0.1 were used. Figure (A1D) shows a situation with $f(H_{ij}) = H_{ij}$ in equation (A4'); it does not have the smooth acceleration shown in Figure (A1A). The same h_{ij} values as for Figure (A1C) were used for this simulation.

The potential of an HC connected to its neighbors through gap junctions is defined by:

$$\frac{dh_{ij}}{dt} = -h_{ij} + \sum_{(p,q)\in N_{ij}^{H}} P_{pqij}(h_{pq} - h_{ij}) + S_{ij}, \qquad \text{(A6)}$$

where P_{pqij} is the permeability between cells at (i, j) and (p, q); namely,

$$P_{pqij} = \frac{-1}{1+\exp[-(|S_{ij} - S_{pq}| - \beta_p)/\lambda_p]} + 1. \qquad \text{(A7)}$$

Terms β_p and λ_p in (A7) are constants, and N^{H}_{ij} in (A6) is the neighborhood of size ϵ_H to which the model HC at (i, j) is connected:

$$N_{ij}^{H} = \left\{(p,q) : \sqrt{(i-p)^2 + (j-q)^2} \le \varepsilon_H \text{ and } (p,q) \ne (i,j)\right\}. \qquad \text{(A8)}$$

Center - Surround Stage

The retinally adapted signal S_{ij} is then processed by small-scale and medium-scale on-center off-surround networks. In the following, scale subscripts (e.g., X_s and X_m for small and medium scales, respectively) are omitted for simplicity. An on-center off-surround network of cell activities X_{ij} that obey membrane equations (Grossberg, 1973, 1980) is defined as follows:

$$\frac{dX_{ij}}{dt} = -AX_{ij} + (B - X_{ij})C_{ij} - (X_{ij} + D)E_{ij}, \qquad \text{(A9)}$$

where A, B and D are constants. The on-center input obeys:

$$C_{ij} = W_E S_{ij}, \qquad \text{(A10)}$$

and the off-surround input obeys:

$$E_{ij} = \left(\sum_{(p,q)\in N_{ij}^{E}} S_{pq} E_{pqij}\right) \frac{W_E}{\sum_{(p,q)\in N_{ij}^{E}} E_{pqij}}, \qquad \text{(A11)}$$

with the inhibitory Gaussian off-surround kernel:

$$E_{pqij} = E\exp\left\{-\frac{(p-i)^2 + (q-j)^2}{\alpha^2}\right\}. \qquad \text{(A12)}$$

Coefficient E in (A12), which normalizes and makes the sum of the surround kernel equal the weight W_E, is defined by:

$$E = \frac{W_E}{\sum_{(p,q)\in N^{E}} \exp\left\{-\frac{p^2 + q^2}{\alpha^2}\right\}}. \qquad \text{(A13)}$$

Terms α and W_E are constants. N_{ij}^{E} in (A11) is the off-surround neighborhood to which the cell at (i, j) is connected:

$$N_{ij}^{E} = \left\{(p,q) : \sqrt{(i-p)^2 + (j-q)^2} \le \varepsilon_E \text{ and } 0 \le p \le 199 \text{ and } 0 \le q \le 199\right\}, \qquad \text{(A14)}$$

where ϵ_E is a constant defining the size of the neighbor. N^E in (A13) is the neighbor for the standard center kernel defined as follows.

$$N^E = \left\{(p,q) : \sqrt{(i-p)^2 + (j-q)^2} \le \varepsilon_E \right\}. \quad \text{(A15)}$$

The only difference between N_{ij}^E and N^E is that N_{ij}^E is constrained by the boundary of the image (200x200), which may cut kernels along the borders, while N^E, which defines the whole kernel, is not.

For each position, the normalizing factor $W_E / \Sigma E_{pqij}$ in (A11) is a constant, mostly just 1, except for the positions along the border of the image. Normalization eliminates unwanted boundary effects created by filters with a fixed kernel size. In case of a center-surround filter, for example, without normalization, halos along the border of the image can occur because of the disinhibition caused by cut kernels there.

The equilibrium activities of (A9) are:

$$X_{ij} = \frac{BC_{ij} - DE_{ij}}{A + C_{ij} + E_{ij}}. \quad \text{(A16)}$$

Luminance signals L_{ij}, which constitute the large-scale of the center-surround process, are defined by:

$$L_{ij} = S_{ij} \quad \text{(A17)}$$

Through these processes, the initial stage of the model achieves automatic gain control in all its small, medium and large scales. Output from the individual scales are pooled to form a multiple-scale output signal as follows:

$$M_{ij} = \left[w_s (X_{ij}^s + b_S) + w_m (X_{ij}^m + b_M) + w_l L_{ij}\right]^+, \quad \text{(A18)}$$

where w_s, w_m, w_l, are weighting constants, and b_S, b_M are tonic bias terms. See Table 1.

Lightness Anchoring

At the anchoring stage, the pooled multiple-scale input M_{ij} becomes anchored into the activity A_{ij} using the membrane equation:

$$\frac{dA_{ij}}{dt} = -B_A A_{ij} + \Psi\left(C_A - A_{ij}\right)M_{ij}, \quad \text{(A19)}$$

where B_A and C_A are constants. The tonic gain control signal Ψ, which modulates all the anchoring activities A_{ij}, uses the membrane equation:

$$\frac{d\Psi}{dt} = \tau_\Psi \left\{-\Psi + \left(B_\Psi - \Psi\right)T_\Psi - \Psi H\right\}. \quad \text{(A20)}$$

Term τ_Ψ is a time constant that determines the speed of integration of (A20). The term $-\Psi$ is a leakage component. A tonic excitatory component T_Ψ drives the gain control signal Ψ toward its maximum B_Ψ until the inhibitory gain control ΨH kicks in by the activation of the suppressive signal H. The suppressive signal H becomes activated when any output of the BHLAW module b_{ij} reaches a threshold to begin the anchoring of a blurred "highest luminance" to white as follows:

$$H = \begin{cases} \varphi & \text{if any } \; b_{ij} \ge \varpi \\ 0 & \text{otherwise,} \end{cases} \quad \text{(A21)}$$

where ϖ and ϕ are constants. Function b_{ij} in (A21) is a blurred version of the anchoring signal A_{ij}:

$$b_{ij} = \sum_{(p,q)\in N_{ij}^{A}} G_{pqij}^{A} A_{pq}, \tag{A22}$$

where the blurring Gaussian anchoring kernel is defined by:

$$G_{pqij}^{A} = G^{A} \exp\left\{-\frac{(p-i)^2+(q-j)^2}{\varsigma_A^2}\right\} \frac{W_A}{\sum_{(p,q)\in N_{ij}^{A}} G_{pqij}^{A}}. \tag{A23}$$

In (A23),

$$G^{A} = \frac{W_A}{\sum_{(p,q)\in N^{A}} \exp\left\{-\frac{p^2+q^2}{\zeta_A^2}\right\}}, \tag{A24}$$

and W_A and ζ_A are constants. The size of the blurring neighborhood N_{ij}^{A} in (A22) is defined as follows:

$$N_{ij}^{A} = \left\{(p,q): \sqrt{(i-p)^2+(j-q)^2} \le \varepsilon_A \text{ and } 0 \le p \le 199 \text{ and } 0 \le q \le 199\right\}, \tag{A25}$$

where ϵ_A is a constant defining the size of the neighbor. N^{A} in equation (A24) is the neighborhood for the standard blurring kernel:

$$N^{A} = \left\{(p,q): \sqrt{(i-p)^2+(j-q)^2} \le \varepsilon_A\right\}. \tag{A26}$$

The final value A_{ij} can be approximated without numerically integrating (A19) – (A26). It is usually the case that the point where the blurred-highest-luminance $\max(\sum_{pqij} G_{pqij}^{A} M_{ij})$ happens gets anchored to white. Thus we can estimate from (A19) the approximation Ψ' of the final value of Ψ, by assuming the following:

$$\varpi = \frac{C_A \Psi'\left(\max \sum_{pq} G_{pqij}^{A} M_{ij}\right)}{B_A + \Psi'\left(\max \sum_{pq} G_{pqij}^{A} M_{ij}\right)}. \tag{A27}$$

This equation modifies the steady state-solution of (A19):

$$A_{ij} = \frac{C_A \Psi M_{ij}}{B_A + \Psi M_{ij}}, \tag{A28}$$

to directly implement the BHLAW rule. The left part of the equation is set to white ϖ, and the pooled multiple-scale M_{ij} is replaced by "blurred highest luminance" $\max(\sum_{pqij} G_{pqij}^{A} M_{ij})$. By rearranging (A27), we get the following result:

$$\Psi' = \frac{B_A \varpi}{\left(\max \sum_{pq} G_{pqij}^{A} M_{ij}\right)(C_A - \varpi)}. \tag{A29}$$

Although Ψ' always closely predicts the real value Ψ, some adjustments can be made to be more accurate. For this, the steady-state value of the predicted anchoring value $A_{ij}^{'}$ given Ψ' needs to be calculated from (A28):

$$A_{ij}^{'} = \frac{C_A \Psi^{'} M_{ij}}{B_A + \Psi^{'} M_{ij}} \ . \qquad \text{(A30)}$$

The final values of the anchored signals A_{ij} are calculated by normalizing the predicted value $A_{ij}^{'}$ as follows:

$$A_{ij} = A_{ij}^{'} \left(\frac{\varpi}{\max \sum_{pq} G_{pqij}^{A} A_{pq}^{'}} \right). \qquad \text{(A31)}$$

The normalizing factor in the parenthesis in equation (A31) assures that the final blurred-highest anchoring value $\max(\sum_{pqij} G_{pqij}^{A} A_{ij})$ equals white ϖ. This shortcut version of anchoring runs at least 100 times faster than the one in equation (A19) by cutting hundreds of numerical integration steps.

Gray-Scale to Color Mapping

To simplify the visual processing, normalized red (R_{ij}^{I}), green (G_{ij}^{I}) and blue (B_{ij}^{I}) color values at each pixel point (i, j) having a range from 0 to 1 are first converted to a luminance input value I_{ij} (Pratt, 1991):

$$I_{ij} = 0.3R_{ij}^{I} + 0.59G_{ij}^{I} + 0.11B_{ij}^{I} \ . \qquad \text{(A32)}$$

In 8-bit color expression having a range from 0 to 255, for example, each color value needs to be divided by 255 for normalization. After calculating the retinal preprocessing stage in equation (A4), the ratio S_{ij}/I_{ij} at each pixel point is calculated as follows:

$$r_{ij}^{SI} = \frac{S_{ij}}{I_{ij}}. \qquad \text{(A33)}$$

Using this ratio r_{ij}^{SI}, the corresponding color ($R_{ij}^{S}, G_{ij}^{S}, B_{ij}^{S}$) values for S_{ij} are calculated as follows:

$$\begin{pmatrix} R_{ij}^{S} \\ G_{ij}^{S} \\ B_{ij}^{S} \end{pmatrix} = r_{ij}^{SI} \begin{pmatrix} R_{ij}^{I} \\ G_{ij}^{I} \\ B_{ij}^{I} \end{pmatrix}. \qquad \text{(A34)}$$

Equations (A33) and (34) convert the first neural signal in the visual pathway into the corresponding color values. These luminance signal and the color signals are used to recover the anchored color lightness in the following.

After calculating the anchored lightness A_{ij} in (A19), the normalized lightness is calculated:

$$A_{ij}^{*} = \frac{A_{ij}}{\varpi}, \qquad \text{(A35)}$$

where the *white* ϖ is the same constant as in (A21) and Figures 4 and 5. Then the ratio between A_{ij}^{*} and S_{ij} is calculated:

$$r_{ij}^{AS} = \frac{A_{ij}^{*}}{S_{ij}}. \qquad \text{(A36)}$$

To express bright red, green and blue values, the ratio r_{ij}^{AS} was divided into a color portion r_{ij}^{AC} and a luminance portion r_{ij}^{AL}. For example, a bright blue with luminance 0.3 may have a near-saturating value for blue (luminance 0.11) as the color portion, and some red and green of an equal value as the luminance part (luminance 0.19). The color part of the ratio is calculated as follows:

$$r_{ij}^{AC} = \Omega\left\{\frac{2}{1+\exp[-(2r_{ij}^{AS}/\Omega)]} - 1\right\}, \qquad \text{(A37)}$$

where Ω is a constant that sets the asymptote (Figure A3). The difference between and r_{ij}^{AC} is taken as a luminance component:

$$r_{ij}^{AL} = r_{ij}^{AS} - r_{ij}^{AC}. \qquad \text{(A38)}$$

Figure A3A illustrates how the model assigns the color and luminance parts for a color representation of the output. The curve corresponds to the color part r_{ij}^{AC} in (A37). The broken line represents the ideal situation where the achromatic luminance and chromatic luminance are always the same ($r_{ij}^{AC} = r_{ij}^{AS}$). The difference between the broken line and the curve is the luminance part r_{ij}^{AL}. Equation (A37) assigns a larger fraction to luminance as the ratio r_{ij}^{AS} increases. Since $r_{ij}^{AS} > 1$ means that the anchored lightness A_{ij}^{*} is larger than the retinally processed signals S_{ij} in (A4), (A37) prevents colors from saturating by increasing the contribution of luminance when the anchored lightness becomes larger than the retinal signal. The two color and luminance channels are combined to define the perceived color:

$$\begin{pmatrix} R_{ij}^{A} \\ G_{ij}^{A} \\ B_{ij}^{A} \end{pmatrix} = r_{ij}^{AC} \begin{pmatrix} R_{ij}^{S} \\ G_{ij}^{S} \\ B_{ij}^{S} \end{pmatrix} + r_{ij}^{AL} \begin{pmatrix} S_{ij} \\ S_{ij} \\ S_{ij} \end{pmatrix}. \qquad \text{(A39)}$$

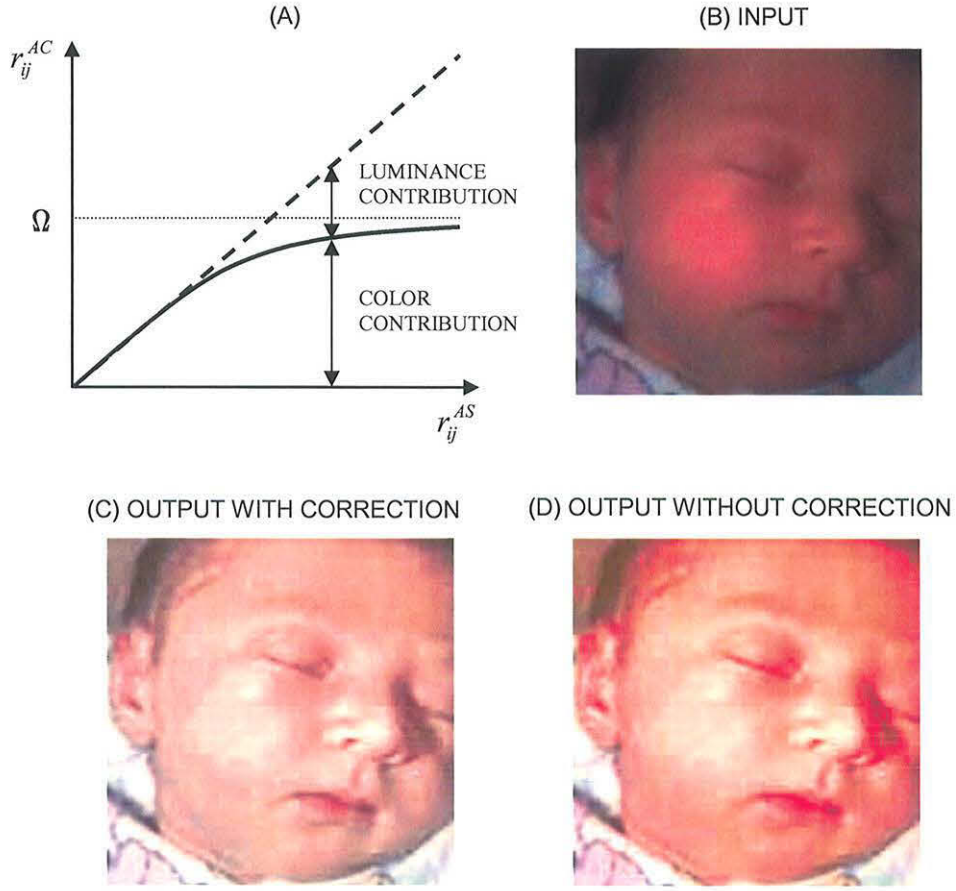

Figure A3. (A) The achromatic luminance is divided into color part (the curve) and luminance part (the difference between the broken line and the curve). The broken line corresponds to $r_{ij}^{AC}=r_{ij}^{AS}$. Ω is the asymptote of the curve. (B) Stimulus. (C) Output of the model. (D) An output without color correction. The output used $r_{ij}^{AC}=r_{ij}^{AS}$ in place of equation (A37). [Figure (B) is reproduced with permission from Kimmel et al. (2003)].

Figure A3C shows an example of model output where the saturation of red has been corrected. Instead of increasing the reddish color value linearly to match the achromatic luminance value, as in Figure A3D, the model properly mixes the corrected color part by (A37) with the complementary luminance part to prevent saturation of red, thereby generating a natural looking output.

Equations (A38) and (A39) assure that the color luminance, defined as

$$A_{ij}^{L}=0.3R_{ij}^{A}+0.59G_{ij}^{A}+0.11B_{ij}^{A}, \qquad \text{(A40)}$$

has the same luminance as the corresponding normalized achromatic luminance A_{ij}^{*}. This fact can be proved as follows. First, using the definition R_{ij}^{A}, G_{ij}^{A} and B_{ij}^{A} in (A39), equation (A40) can be rewritten as follows:

$$A_{ij}^{L} = 0.3\left(r_{ij}^{AC} R_{ij}^{S} + r_{ij}^{AL} S_{ij}\right) + 0.59\left(r_{ij}^{AC} G_{ij}^{S} + r_{ij}^{AL} S_{ij}\right) + 0.11\left(r_{ij}^{AC} B_{ij}^{S} + r_{ij}^{AL} S_{ij}\right). \quad \text{(A41)}$$

By rearranging, it becomes

$$A_{ij}^{L} = \left\{0.3 r_{ij}^{AC} R_{ij}^{S} + 0.59 r_{ij}^{AC} G_{ij}^{S} + 0.11 r_{ij}^{AC} B_{ij}^{S}\right\} + r_{ij}^{AL} S_{ij}. \quad \text{(A42)}$$

The color luminance in (A42) includes the contributions by the color part (the terms in the bracket) and the luminance part (the last term). For the normalized achromatic luminance A_{ij}^{*}, an identical form as (A42) can be derived. First, by combining equations (A32), (A33) and (A34) we can show the following relationship:

$$S_{ij} = 0.3 R_{ij}^{S} + 0.59 G_{ij}^{S} + 0.11 B_{ij}^{S}, \quad \text{(A43)}$$

A combination and rearrangement of equations (A36) and (A43) leads to the following:

$$A_{ij}^{*} = 0.3 r_{ij}^{AS} R_{ij}^{S} + 0.59 r_{ij}^{AS} G_{ij}^{S} + 0.11 r_{ij}^{AS} B_{ij}^{S}. \quad \text{(A44)}$$

Equation (A44) can be rewritten as follows:

$$\begin{aligned} A_{ij}^{*} = {} & 0.3\left(r_{ij}^{AC} + r_{ij}^{AS} - r_{ij}^{AC}\right) R_{ij}^{S} + 0.59\left(r_{ij}^{AC} + r_{ij}^{AS} - r_{ij}^{AC}\right) G_{ij}^{S} \\ & + 0.11\left(r_{ij}^{AC} + r_{ij}^{AS} - r_{ij}^{AC}\right) B_{ij}^{S}. \end{aligned} \quad \text{(A45)}$$

A rearrangement of (A45) leads to:

$$\begin{aligned} A_{ij}^{*} = {} & \left\{0.3 r_{ij}^{AC} R_{ij}^{S} + 0.59 r_{ij}^{AC} G_{ij}^{S} + 0.11 r_{ij}^{AC} B_{ij}^{S}\right\} \\ & + \left(r_{ij}^{AS} - r_{ij}^{AC}\right)\left\{0.3 R_{ij}^{S} + 0.59 G_{ij}^{S} + 0.11 B_{ij}^{S}\right\}. \end{aligned} \quad \text{(A46)}$$

Using the relationships in (A38) and (A43), equation (A46) can be rewritten as follows:

$$A_{ij}^{*} = \left\{0.3 r_{ij}^{AC} R_{ij}^{S} + 0.59 r_{ij}^{AC} G_{ij}^{S} + 0.11 r_{ij}^{AC} B_{ij}^{S}\right\} + r_{ij}^{AL} S_{ij}. \quad \text{(A47)}$$

Notice that A_{ij}^{L} in (A42) is the same as A_{ij}^{*} in (A47), proving that the color luminance and the corresponding achromatic luminance are the same.

When there is a value bigger than 1 in any of R_{ij}^{A}, G_{ij}^{A} and B_{ij}^{A}, the value is truncated to 1, and no more correction is performed.

Appendix B

The stimuli used to generate the shift property of the retinal sensitivity in Figure 2B were generated by the following formula:

$$I_{ij} = \rho_{ij} E_{ij}, \tag{B1}$$

where I_{ij} is the luminance at position (i, j), ρ_{ij} is the reflectance at point (i, j), and E_{ij} is the illumination of (i, j) (Hurlbert, 1989). For a given stimulus, E_{ij} was chosen to be uniform across the image. To examine the full dynamic profile of the shift property, the range of ρ_{ij} was chosen to be –4 to 5 in log-scale for a fixed illumination level. See Figure 2B for the values of illumination E_{ij} used for the simulations.

For all other stimuli used in the paper except for the stimulus in Figure 7, equation (B1) with $E_{ij} = 1$ was used. For the stimulus in Figure 7, the following equations are used:

$$\begin{cases} \rho_{ij} = 0.3, & \text{if } (40 < i < 70 \text{ and } 85 < j < 115), \\ & \text{or if } (130 < i < 160 \text{ and } 85 < j < 115) \\ \rho_{ij} = 0.1, & \text{otherwise.} \end{cases} \tag{B2}$$

and

$$E_{ij} = 1 + \frac{1}{125} i. \tag{B3}$$

Appendix C

The relationship between the size of the connected neighborhood in equation (A8) and the speed of diffusion in equation (A6) is measured using a 50x50 two-dimensional (i, j) grid where the diffusive process is unimpeded.

Before the diffusive process (at $t = 0$), a test stimulus (INPUT in Figure 16B) that has signals only at the rightmost part of the square is loaded to the diffusive layer as follows:

$$h_{ij}(0) = \begin{cases} 0.5 & \text{if } 36 \le i \le 50 \\ 0 & \text{otherwise.} \end{cases} \qquad \text{(C1)}$$

The white region of INPUT in Figure 16B indicates the active portion. The units in (A6) then go through an unimpeded diffusion (the permeabilities $P_{pqij} = 1$):

$$\frac{dh_{ij}}{dt} = \sum_{(p,q)\in N_{ij}^{H}} (h_{pq} - h_{ij}) \ , \qquad \text{(C2)}$$

where neighborhood N_{ij}^{H} is defined in (A8). When the grid is "filled-in", the process (C2) is terminated. The criterion of filled-in is when the leftmost column of the square grid becomes as active as 95% of the rightmost column of the grid. This criterion is chosen to make a convincingly homogeneous spread of signals. The size of the connected neighborhood ϵ_H in A(9), which corresponds to "SIZE OF NEIGHBORHOOD" in Figure 16B, varied from 1 to 15. The number of iterations of numerical integration needed to fill-in the grid was measured for each ϵ_H.

References

Agostini, T., & Castellarin I. (2003). Interaction of chromatic and achromatic surfaces in lightness perception. *Vision Sciences Society, Third Annual Meeting, Sarasota, Florida*. pp. 120 (abstract).

Barlow, H.B., & Levick, W.R. (1969). Three factors limiting the reliable detection of light by retinal ganglion cells of the cat. *Journal of Physiology*, **200**, 1-24.

Bressan, P. (2001), Explaining lightness illusions. *Perception*, **30**, 1031-1046.

Carpenter, G., & Grossberg, S. (1981). Adaptation and transmitter gating in vertebrate photoreceptors. *Journal of Theoretical Neurobiology*, **1**, 1-42. Reprinted in Grossberg, S. (1987), *The adaptive brain*, Volume 1, Amsterdam: Elsevier/North Holland.

Cohen, M.A., & Grossberg, S. (1984). Neural dynamics of brightness perception: features, boundaries, diffusion, and resonance. *Perception & Psychophysics*, **36**, 428-456.

Cole, R.E., & Diamond, A.L. (1971). Amount of surround and test inducing separation in simultaneous brightness contrast. *Perception & Psychophysics*, **9**, 125-128.

Dolan, R.P., & Schiller, P.H. (1994). Effects of ON channel blockade with 2-amino-4-phosphonobutyrate (APB) on brightness and contrast perception in monkeys. *Visual Neuroscience*, **11**, 23-32.

Dowling, J.E. (1987). The Retina: An approachable part of the brain. (Cambridge, MA; Harvard University Press).

Enroth-Cugell, C., & Shapley, R.M. (1973). Adaptation and dynamics of cat retinal ganglion cells. *Journal of Physiology*, **233**, 271–309.

Fahrenfort, I., Habets, R.L., Spekreijse, H., & Kamermans, M. (1999). Intrinsic cone adaptation modulates feedback efficiency from horizontal cells to cones. *Journal of General Physiology*, **114**, 511-24.

Fain, G.L. (2001) Dark adaptation. *Progress in Brain Research*, **131**, 383-394.

Fry, G.A., & Alpern, M. (1953). The effect of a peripheral glare source upon the apparent brightness of an object. *Journal of the Optical Society of America*, **43**, 189-195.

Gilchrist, A.L., Kossyfidis, C., Bonato, F., Agostini, T., Cataliotti, J., Li, X., Spehar, B., Annan, V., & Economou, E. (1999). An anchoring theory of lightness perception. *Psychological Review*, **106**, 795-834.

Grossberg, S. (1973). Contour enhancement, short term memory, and constancies in reverberating neural networks. *Studies in Applied Mathematics,* **52**, 213-257.

Grossberg, S. (1980). How does a brain build a cognitive code? *Psychological Review*, **87**, 1-51.

Grossberg, S. (1983). The quantized geometry of visual space: The coherent computation of depth, form and lightness. *Behavioral & Brain Sciences*, **6**, 625-692.

Grossberg, S. (1994). 3-D vision and figure-ground separation by visual cortex. *Perception & Psychophysics*, **55**, 48-120.

Grossberg, S., & Hong, S. (2003). A neural model of surface perception: lightness, anchoring, and filling-in. Submitted for publication.

Grossberg, S., Mingolla, E., & Williamson, J. (1995). Synthetic aperture radar processing by a multiple scale neural system for boundary and surface representation. *Neural Networks*, **7/8**, 1005-1028.

Grossberg, S., & Todorović, D. (1988). Neural dynamics of 1-D and 2-D brightness perception: a unified model of classical and recent phenomena. *Perception & Psychophysics*, **43**, 241–277.

Helmholtz, H. von, (1866). *Helmholtz's treatise on physiological optics*, New York: Optical Society of America.

Hong, S., & Grossberg, S. (2003). Cortical Dynamics of Surface Lightness Anchoring, Filling-In, and Perception. *Vision Sciences Society, Third Annual Meeting, Sarasota, Florida*. pp. 120.

Horn, B.K.P. (1977). Understanding image intensities. *Artificial Intelligence*, **21**, 201-231.

Hurlbert, A.C. (1989). *The computation of color.* Doctoral thesis. MIT.

Jobson, D.J., & Woodell, G.A. (1995). Properties of a Center/Surround Retinex: Part 2. Surround Design. *NASA Technical Memorandum, 110188.*

Kamermans, M., Haak, J., Habraken, JB., & Spekreijse, H. (1996). The size of the horizontal cell receptive fields adapts to the stimulus in the light adapted goldfish retina. *Vision Research*, **36**, 4105-4119.

Kimmel, R., Elad, M., Shaked, D., Keshet, R. & Sobel, I. (2003). A Variational Framework for Retinex. *The International Journal on Computer Vision*, **52**, 7-23.

Koutalos, Y., & Yau, K.W. (1996). Regulation of sensitivity in vertebrate rod photoreceptors by calcium. *Trends in Neurosciences*, **19** , 73-81.

Land, E.H., & McCann, J.J. (1971). Lightness and Retinex theory. *Journal of the Optical Society of America*, **61**, 1-11.

Lee, B.B., Dacey, D.M., Smith, V.C., & Pokorny, J. (1999). Horizontal cells reveal cone type-specific adaptation in primate retina. *Proceedings of the National Academy of Sciences U S A*, **96**, 14611-14616.

Leibowitz, H. Mote, F.A. & Thurlow, W.R. (1953). Simultaneous contrast as a function of separation between test and inducing fields. *Journal of Experimental Psychology*, **46**, 453-456.

McMahon, D.G., Zhang, D.Q., Ponomareva, L., & Wagner, T. (2001). Synaptic mechanisms of network adaptation in horizontal cells. *Progress in Brain Research*, **131**, 419-436

Mills, S.L., & Massey, S.C. (1995). Differential properties of two gap junctional pathways made by AII amacrine cells. *Nature*, **377**, 734-737.

Mingolla, E., Ross, W., & Grossberg, S., (1999). A neural network for enhancing boundaries and surfaces in synthetic aperture radar images. *Neural Networks*, **12**, 499-511.

Nawy, S. (2000). Regulation of the on bipolar cell mGluR6 pathway by Ca^{2+}. *Journal of Neuroscience*, **20**, 4471-4479

Newson, L.J. (1958). Some principles governing changes in the apparent lightness of test surfaces isolated from their normal backgrounds. *Quarterly Journal of Experimental Psychology*, **10**, 82-95.

Normann, R.A., & Perlman I. (1979). The effects of background illumination on the photoresponses of red and green cones. *Journal of Physiology*, **286**, 491-507.

Perlman, I., & Normann R.A. (1998). Light adaptation and sensitivity controlling mechanisms in vertebrate photoreceptors. *Progress in retinal and eye research*, **17**, 523-563.

Perona, P., Malik, J., (1990). Scale-space and edge detection using anisotropic diffusion, *IEEE Transactions on Pattern Analysis and Machine Intelligence*, **12**, 629-639.

Pessoa, L., Mingolla, E., & Neumann, H. (1995). A contrast- and luminance-driven multiscale network model of brightness perception. *Vision Research*, **35**, 2201-2223.

Pratt, W.K. (1991). Digital image processing, *John Wiley & Sons*, 2nd edition, New York,

Rahman, Z., Jobson, D.J., & Woodell, G.A. (1996). Multiscale Retinex for Color Image Enhancement. *International Conference on Image Processing (ICIP) '96.*

Rahman, Z., Woodell, G.A. & Jobson, D.J. (1997). A Comparison of the Multiscale Retinex With Other Image Enhancement Techniques. *Proceedings of the IS&T 50th Anniversary Conference.*

Ribelayga, C., Wang, Y., & Mangel, S.C. (2002). Dopamine mediates circadian clock regulation of rod and cone input to fish retinal horizontal cells. *Journal of Physiology*, **544**, 801-816.

Schiller, P.H. (1992). The ON and OFF channels of the visual system. *Trends in Neurosciences*, **15**, 86-92.

Schiller, P.H., Sandell, J.H., & Maunsell, J.H. (1986). Functions of the ON and OFF channels of the visual system. *Nature*, **322**, 824-825.

Sterling, P. (1998). Retina. In G. M. Shepherd, (Ed.), *The Synaptic Organization of the Brain*, Volume 4 (pp. 205-253), New York: Oxford University Press.

Thibos, L.N., & Werblin, F.S. (1978). The response properties of the steady antagonistic surround in the mudpuppy retina. *Journal of Physiology*, **278**, 79-99.

Verweij, J., Kamermans, M., & Spekreijse, H. (1996). Horizontal cells feed back to cones by shifting the cone calcium-current activation range. *Vision Research*, **36**, 3943-3953.

Wallach, H. (1948). Brightness constancy and the nature of achromatic colors. *Journal of Experimental Psychology*, **38**, 310-324.

Wallach, H. (1976). *On perception*, New York: Quadrangle/The New Your Times Book Co.

Waxman, A.M., Gove, A.N., Fay, D.A., Racamato, J.P., Carrick, J.E., Seibert, M.C. & Savoye, E.D. (1997). Color night vision – opponent processing in the fusion of visible and IR imagery. *Neural Networks*, **10**, 1-6.

Werblin, F.S. (1971). Adaptation in a vertebrate retina: intracellular recording in Necturus. *Journal of Neurophysiology*, **34**, 228-241.

Werblin, F.S. (1974). Control of retinal sensitivity. II. Lateral interactions at the outer plexiform layer. *Journal of General Physiology*, **63**, 62-87.